Journal of Geophysical Research: Earth Surface

RESEARCH ARTICLE
10.1029/2018JF004857

Intertidal Area Disappears Under Sea Level Rise: 250 Years of Morphodynamic Modeling in San Pablo Bay, California

H. Elmilady[1,2,3], M. van der Wegen[1,2], D. Roelvink[1,2,3], and B. E. Jaffe[4]

[1]IHE-Delft Institute for Water Education, Delft, Netherlands, [2]Deltares, Delft, Netherlands, [3]Civil Engineering and Geosciences, Delft University of Technology, Delft, Netherlands, [4]USGS Pacific Coastal and Marine Science Center, Santa Cruz, CA, USA

Key Points:
- 3-D, process-based model hindcasts 150 years of morphodynamic development in subembayment of San Francisco Bay with significant skill
- Forecasts show that the mudflats drown under 100-year sea level rise scenarios despite net deposition
- Model results suggest that estuarine intertidal area is at stake under anticipated sea level rise scenarios

Supporting Information:
- Supporting Information S1
- Figure S1

Correspondence to:
H. Elmilady,
h.elmilady@un-ihe.org

Citation:
Elmilady, H., van der Wegen, M., Roelvink, D., & Jaffe, B. E. (2019). Intertidal area disappears under sea level rise: 250 years of morphodynamic modeling in San Pablo Bay, California. *Journal of Geophysical Research: Earth Surface, 124*, 38–59. https://doi.org/10.1029/2018JF004857

Received 28 AUG 2018
Accepted 8 DEC 2018
Accepted article online 12 DEC 2018
Published online 10 JAN 2019

Abstract Anticipated sea level rise (SLR) threatens intertidal areas and associated ecosystems in estuaries worldwide. There is a need to develop validated modeling tools to assess the impact of SLR on estuarine morphodynamics. This study explores the morphological impact of SLR on a channel-shoal system in San Pablo Bay, a subembayment of San Francisco Bay, California, using a 3-D, process-based modeling approach (Delft3D) including density currents and wave action. The Bay underwent considerable morphologic development in response to variations in fluvial sediment load and discharge associated with a period of hydraulic mining for gold and later damming in the watershed. The availability of a unique 150-year, 30-year sequenced, bathymetric data set provided a rare opportunity for model validation. We investigate a 250-year period of morphodynamic evolution including a 150-year hindcast and a 100-year forecast with different SLR scenarios. The model shows significant skill in hindcasting volumes and patterns of bathymetric development during both net depositional (1856–1951) and erosional (1951–onward) periods. Forecasts show that SLR alters the Bay's erosional trend to a depositional trend again. Despite increased sediment trapping rates, the intertidal mudflats drown under all modeled SLR scenarios (42, 84, and 167 cm by end of the 21st century). Our work highlights the potential of using process-based models to assess the morphodynamic impact of SLR. The study also suggests that SLR can greatly increase the loss of intertidal area when landward migration is not possible. Sustainable management strategies are required to safeguard these valuable intertidal habitats.

Plain Language Summary Sea level rise is expected to affect coastal areas all around the world including the estuarine environment. In particular, the estuarine intertidal area comprises delicate and valuable ecosystems. Anticipated sea level rise poses questions on the fate of this unique estuarine environment. In this research, we aim to validate a numerical model against observed bed level developments in San Pablo Bay, a subembayment of San Francisco Estuary, to make trustworthy predictions of the estuarine bed including future sea level rise. The model included detailed tidal water movement, wind-wave action, sediment transports, and resulting bed level updates. Our hindcast (1856–1983) showed significant skill in reproducing observed bed level developments. Our forecast shows that sea level rise slowly drowns the intertidal environment. The sea level rise rate is larger than the accretion rate of the mudflats. Mitigation and adaptation strategies are required to ensure the sustainability of the estuarine environment against climate-induced changes.

1. Introduction

Estuaries are the transition zones between land and sea where the interaction between freshwater and tidally varying saline water makes it one of the most productive ecosystems in the world (Harvey et al., 1998). The estuarine bed has a dynamic nature and is subject to marine (e.g., waves, tides, salinity, and sea level) and fluvial (e.g., discharges and sediment load) forcing. Sediments may have local, fluvial, or marine origin and shape the estuarine morphology into channels, shoals, and intertidal area. This morphology forms the basis for valuable estuarine habitat and ecosystems (Harvey et al., 1998). Maintaining this diverse nature is crucial for ensuring the estuarine sustainability. Constant hydrodynamic and sedimentological forcing leads to morphological equilibrium over a time scale longer than decades (Dam et al., 2016; van der Wegen & Roelvink, 2008). However, changes in forcing conditions lead to continuous morphological adaptations ranging from seasons to millennia (e.g., Pethick, 1994; van der Wegen et al., 2016).

Throughout history, natural forcing perturbations occurred and the estuarine morphology adapted accordingly. Sea level fluctuated in accordance with Earth's climate and reached its modern levels from about

6,000 years ago (Fleming et al., 1998). Between 1 and 1800 CE, there were relatively slight sea level changes. However, sea level began to rapidly rise in the nineteenth century and further accelerated in the early twentieth century. Currently, the sea level rise (SLR) rate is much greater than any time in the past 200 years (Kemp et al., 2011) and global SLR projections range from 0.2 m to approximately 2.0 m by the end of the 21st century (Parris et al., 2012).

Estuaries must accrete by trapping sediment in order to keep up with the rising sea level (Castagno et al., 2018; Fagherazzi et al., 2013; Leonardi et al., 2018). The current accelerated SLR is expected to have a slow, potentially governing impact on the future state of estuarine systems. Examples are shoreline erosion (Passeri et al., 2015), loss of salt marshes, and coastal wetlands along with their associated habitats (Nicholls & Cazenave, 2010; Sampath et al., 2011; Thorne et al., 2018), coastal squeeze and increased inundation and flooding (Pelling & Blackburn, 2013), decline of intertidal area (Rossington & Spearman, 2009; van der Wegen et al., 2016), and economic losses due to disruption of economic activities or land loss (Asuncion & Lee, 2017; Peri & Šverko, 2015).

Estuaries provide the economic livelihood for several communities (Mitsch & Gosselink, 2000). Human-induced pressure can be seen in estuaries through several aspects such as lack of accommodation space, flow-regulating structures, land reclamations, dredging operations, and ecosystem manipulation (Cooper, 2003). A solid understanding of SLR impact on the morphological state of estuaries is critical for identifying potential threats and associated adaptation measures. Predicting SLR impact on the long-term morphological evolution is challenging as anticipated SLR rates are historically unprecedented and are associated with high uncertainties which require a solid comprehension of the estuarine system dynamics (Sampath et al., 2011).

1.1. Previous Studies

Roughly, behavior-based and process-based models are the two main approaches used in long-term morphodynamic modeling (de Vriend et al., 1993; Murray, 2003; Werner, 2003). Behavior-based models are based on empirical relationships developed from measurements and observations which are extrapolated to address conditions under SLR. Sampath et al. (2011, Guadiana Estuary), Rossington and Spearman (2009, Thames Estuary), and Van Goor et al. (2003) provide examples of behavior-oriented modeling to study SLR impact on estuarine morphodynamics. Their work showed that SLR potentially affects the estuarine morphology more than any other developments in recent history, including, for example, the drowning of intertidal area despite local accretion. This modeling approach does not provide an understanding of the underlying physical mechanisms instead it is based on a combination of expert analysis and empirical relationships developed from observations.

Process-based models take detailed description of physical processes as a starting point. Z. Zhou et al. (2015) implemented a 1-D fundamental approach to investigate the morphological evolution of intertidal flats and sediment sorting dynamics. Van der Wegen and Roelvink (2008) showed millennial time scale 2-D morphodynamic developments using highly schematized conditions in a rectangular embayment. Other implementations of 2-D or 3-D process-based modeling efforts with considerable skill in hindcasting observed bathymetric developments are Dam et al. (2016) for the Western Scheldt (110 years), Ganju et al. (2009) for Suisun Bay (30 years), and van der Wegen, Jaffe, and Roelvink (2011) and van der Wegen and Jaffe (2013) for San Pablo Bay (30 years). In addition to reproducing the morphological evolution, models can be used as virtual labs to perform various investigations of interest. X. Zhou et al. (2013) implemented this approach to investigate the impact of SLR on the long-term morphological development of the Yangtze Estuary. Van der Wegen et al. (2016) used a 1-D model to reproduce a mudflat profile in South San Francisco Bay and quantify the impact of a 100-year SLR. Van der Wegen (2013) evaluated the morphodynamic impact of SLR on a schematic 2-D rectangular tidal basin. Ganju and Schoellhamer (2010) performed a decadal time scale (30 years) morphological forecast for Suisun Bay under different SLR, sediment supply, and river flow scenarios. In all of the above SLR studies, the estuarine morphology experienced notable development and the intertidal area gradually declines.

Previous research provides a solid understanding of the morphological development of the period under consideration and the system's governing processes. However, most previous case studies investigated periods with a time scale that ranges from years to decades. Also, usually the different periods (e.g.,

Depositional/Erosional) were treated in a relatively separate way such as the use of different parameters. In this study, we use the 3-D process-based model applied by van der Wegen, Jaffe, and Roelvink (2011) to investigate the morphological development of San Pablo Bay over a 250-year period incorporating both a validated hindcast from 1856 to 1983 (last available survey) and a SLR forecast from 1983 to 2103. Studying the system on a longer time scale allows for achieving a wider perspective on the morphodynamic evolution and the potential impact of SLR. Our research combines the findings of shorter time scale previous studies into one model in order to produce the first 100-year morphological forecast for San Pablo Bay.

1.2. Research Objective

The aim of this study is to assess the impact of SLR on the long-term morphological development of an estuarine channel-shoal system. San Pablo Bay, a subembayment of San Francisco Estuary, was chosen as a case study due to the availability of a unique historic bathymetric data set that captures the considerable morphological changes over the past 150 years (Jaffe et al., 2007). The data set is used to validate a morphodynamic model hindcast over the past 150 years and to forecast 100 years under SLR scenarios. Our aim is to provide a reliable morphological forecast for the system which will help identify and understand the potential threat of SLR. We apply the process-based, numerical model Delft3D (D3D; Deltares, 2016; Lesser et al., 2004) to compute detailed hydrodynamics, sediment dynamics, and associated morphodynamic development. This research tests the ability of process-based models to predict representable morphological development and provide a methodology for performing such forecasts on a centennial time scale.

2. Case Study

2.1. Setting

San Francisco Estuary is the largest estuary on the west coast of the United States. Its watershed covers more than 195,000 km^2 (US EPA, 2018) and drains about 40% of California State (Kimmerer, 2004). The present-day estuarine configuration with its complex topographical and geological features is a tectonically reshaped river valley which started gradually drowning with SLR since the last ice age (Atwater et al., 1977).

The San Francisco estuarine system is commonly referred to as the Bay-Delta system which comprises both San Francisco Bay and Sacramento-San Joaquin Delta (Figure 1). This system starts inland with two main river branches, the Sacramento and San Joaquin Rivers that drain the enormous watershed through a complex network of tributaries. Following that water flows to the Sacramento-San Joaquin Delta, the only inland Delta in the world (US EPA, 2018), which is located at the confluence zone between both major rivers. Eventually, fresh water gets discharged into San Francisco Bay where it passes through a series of subembayments heading toward the mouth of the estuary at the Golden gate bridge. Starting landward from the Delta there is Suisun Bay followed by San Pablo Bay to the west, then Central Bay to the south in front of Golden Gate, and finally there is South Bay located more to the south of Central Bay. In this research, we model North San Francisco Bay (supporting information Figure S1) which comprises both Suisun Bay and San Pablo Bay along with their only connection through Carquinez Strait.

2.2. Morphology

San Pablo Bay (Figure 1), a subembayment of North San Francisco Bay, is bound by San Pablo Strait to the west and Carquinez Strait to the east. It covers an area of approximately 300 km^2 comprising a channel-shoal system which consists of shoals ($<$5 m MLLW, Mean Lower Low Water) dissected by a deep main channel with a depth larger than 12 m MLLW (Schoellhamer et al., 2008). This channel serves as the main shipping channel as it provides the connection between the deep San Pablo Strait and Carquinez Strait. The surrounding Northern and Southern shoals occupy most of the Bay area accounting for about 190 and 43 km^2, respectively (Bever & MacWilliams, 2013). A small secondary navigation channel bisects the northern shoals and joins to the Petaluma River (Schoellhamer et al., 2008). Throughout this paper, the terms "channel" and "secondary channel" refer to the main and secondary channel, respectively. The Petaluma River and Sonoma Creek are the two main tributaries that flow into San Pablo Bay. San Pablo Bay margins comprise large intertidal mudflats which are in some locations bound by salt marshes.

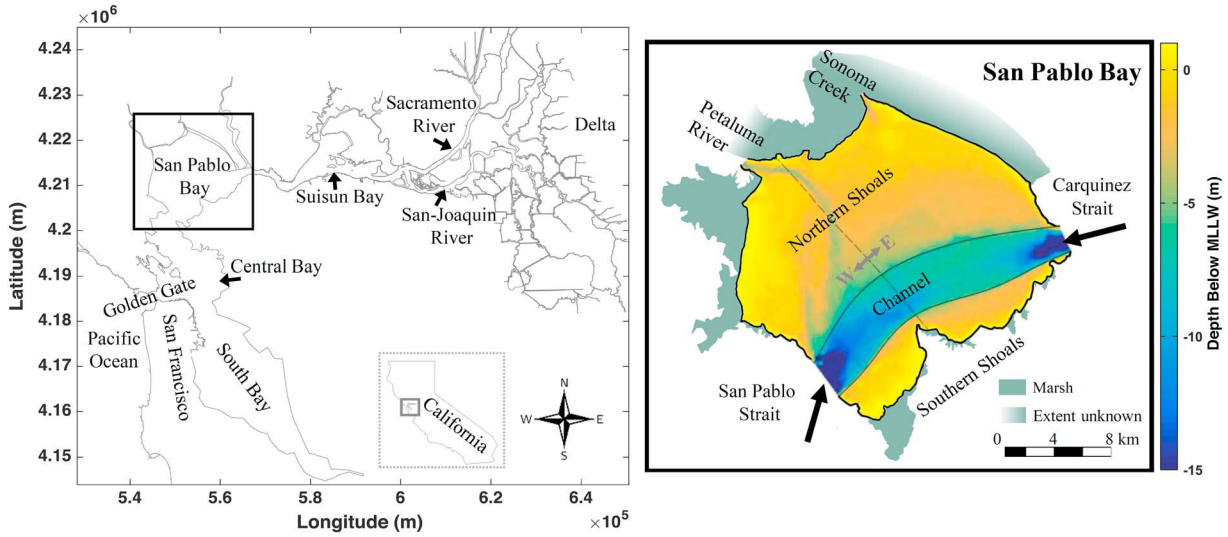

Figure 1. Left panel shows San Francisco Estuary land-boundary. Right panel shows a zoom on San Pablo Bay with its 1856 bathymetry and marsh extent plotted, the thin black line indicates the main channel while the gray dotted line in the middle donates the division used in this study between the eastern and western side of San Pablo Bay.

Carquinez Strait extends about 11 km from Carquinez Bridge at the eastern boundary of San Pablo Bay till Benicia Bridge at the western boundary of Suisun Bay. Its morphology is characterized by a deep channel (max. depth 35 m), steep bed level slopes, a narrow cross-section (≈1,000 m wide), multiple bends, and rocky banks. When entering Suisun Bay, Carquinez Strait splits into two navigational channels, the Northern Channel that extends northeast toward Grizzly Bay and the Southern Channel that extends east-northeast toward the Delta (Ganju & Schoellhamer, 2008). Shoals cover more than 50% of Suisun Bay and can be found in-between and surrounding the two channels and in Honker and Grizzly Bays (Ganju & Schoellhamer, 2006). Similar to San Pablo Bay, a large portion of Suisun Bay shoals are intertidal mudflats bound by salt marshes.

2.3. Tides

San Francisco Bay has a mixed semidiurnal tidal signal, with a median tidal range of approximately 1.8 m (Kimmerer, 2004). In San Pablo Bay, the tidal range can reach about 2.5 m during spring tides and about 1 m during neap tides (Bever & MacWilliams, 2013). The tidal wave propagates from the Pacific Ocean through the Golden Gate into Central Bay then toward San Pablo Bay. Within North Bay, which includes San Pablo Bay, Carquinez Strait, and Suisun Bay, the tidal wave is a progressive wave. Going upstream, the tidal amplitude starts gradually diminishing due to frictional effects, shoreline interaction, and river discharge attenuation. During periods of low discharge, the tide can propagate far upstream, while during high discharges the tide is dampened out at Sacramento (Kimmerer, 2004). Simulations of Achete et al. (2017) showed that SLR will impact the tidal prism and tidal wave penetration. The decreased effect of the bottom friction resulted in further tidal wave penetration in the Delta. The tidal prism increased (≈5%) due to higher flow velocities and slight changes in the net discharge.

2.4. Salinity

Analysis of water quality samples (USGS, 2018) showed that salinity levels within San Pablo Bay channel can be as high as 30 psu during extreme dry conditions such as the 2012–2015 period and as low as about 10 psu during extreme wet conditions such as in year 1997 and 2017. Furthermore, the deep nature of the main channel enhances the formation of salinity stratification during high river flow conditions reaching about 15 psu within the vertical water column during a 2017 peak flow event. During dry conditions, a vertically well-mixed, longitudinal salinity gradient exists between San Pablo and Suisun Bay. This gradient drives gravitational circulation and associated exchange processes between the two subembayments through Carquinez Strait (e.g., Elmilady, 2016).

2.5. River Inflow

San Francisco Bay is fed by both the Sacramento and San Joaquin rivers which account for about 80% and 10–15% of the total annual discharge, respectively (Barnard et al., 2013; Kimmerer, 2004), the remaining discharge is supplied from minor tributaries. The freshwater flow is highest during the winter-spring period (wet season) and lowest during the summer-fall period (dry season). There is a high seasonal and annual variability with peak flows during the wet season reaching as high as 16,000 m^3/s and as low as 300 m^3/s during the dry season (Kimmerer, 2004).

River discharges changed considerably during the past century due to anthropogenic influence. From 1910 to 1975, the Delta and watershed were modified by enhanced channel conveyance, land reclamation, construction of several flow regulation structures, export facilities, and dikes (Barnard et al., 2013). During this period, freshwater discharges were affected significantly especially during the wet season. Currently, the values and timing of discharges are artificially controlled with a series of flow-regulating structures so that the location of the 2 psu isohaline does not retreat landward further than the Sacramento and San Joaquin rivers convergence zone (Kimmerer, 2004). Water is stored in Delta reservoirs during the wet season and released during the dry season to satisfy the fresh water demand and control the salinity levels in the Delta for ecological and agricultural purposes.

Climatic changes are expected to affect riverine flows (IPCC, 2013). Knowles and Cayan (2002) show that in San Francisco Bay watershed, river discharges at the end of the 21st century are expected to increase slightly during the wet seasons with higher runoff peaks and decrease during the dry season compared to the present-day situation. Annual flow volume is expected to remain steady or slightly decline due to a decrease in snowmelt contribution and unimpaired runoff (Cloern et al., 2011).

2.6. Waves and Wind

Locally generated wind-waves play a significant role in shaping the morphology of San Francisco Bay, especially at the muddy shoals (e.g., Ganju et al., 2009; van der Wegen et al., 2016; van der Wegen & Jaffe, 2014). Bever and MacWilliams (2013) show the significant role that wind-generated waves play in the resuspension of sediment and elevating the SSC (Suspended Sediment Concentration) in both the relatively deep and shallow portions of San Pablo Bay. Schoellhamer et al. (2008) observed up to 0.6 m (4 s period) wind-waves in San Pablo Bay with 700 mg/L SSC while 0.2 m waves resulted in a SSC of 200 mg/L. In addition to causing sediment resuspension, wave-induced bed shear stress can lead to high SSC vertical gradients and formation of sediment-induced stratification (MacVean & Lacy, 2014).

The complex topography surrounding North Bay is a strong control on meteorological conditions. The seasonal variability of wind directions in San Pablo Bay can be represented by a western and south-western dominant wind direction (wet/dry season) along with an eastern and south-eastern secondary wind direction (dry season; Hayes et al., 1984; NOAA, 2018; Windfinder, 2018). The average wind speed (2011–2018) is about 4.5 m/s with higher speeds associated with the dominant wind direction (Windfinder, 2018). Maximum sustained wind speed can reach up to 24 m/s (Weather2, 2018). Typically, there is little to no wind during the night.

2.7. Sediment Characteristics

Within North Bay, the sediment size distribution has a high correlation with the local geometry and topography. Fine cohesive sediment (mud) persists at the shoals, while sandy sediment is usually found in and around deep channels (e.g., Conomos & Peterson, 1977; Kimmerer, 2004). This is attributed to the high tidal currents in the channels that causes tidal scouring, while relatively low flow velocities at the shallow zones allow for mud deposition. Locke (1971) reported that more than 90% of the shallow tidal flats in San Pablo Bay are covered with mud, and dynamic patches of mud partly cover the sandy channel.

2.8. Sediment Load

The Sacramento-San Joaquin Delta has supplied most sediment to North Bay (Krone, 1979; B. J. Smith, 1965; Wright & Schoellhamer, 2004), although in recent years the impact of local tributaries increased (Lewicki & McKee, 2010; McKee et al., 2013; Moftakhari et al., 2015). Sediment supplied from the Delta partly deposits on the mudflats in Suisun Bay and San Pablo Bay, while wind-wave-driven resuspension events may further enhance seaward transport (Krone, 1979, 1996). During high river flow events sediment can be directly

transported to the ocean resulting in turbid plumes seaward of the Golden gate (Ruhl & Schoellhamer, 2004). The sediment fluxes through Golden Gate show an ebb-dominated system with a clear net seaward sediment transport (Elias & Hansen, 2013; Erikson et al., 2013; Teeter et al., 1997).

Sediment load to the Bay has changed significantly over the past centuries (Ganju et al., 2008; Gilbert, 1917). Natural variations in precipitation patterns played a role (Goman & Wells, 2000), but human interventions dominated the sediment supply variations. Moftakhari et al. (2015) estimates that about 55% of the 1,500 ± 400 million ton delivered to the estuary from 1849 to 2015 was caused by anthropogenic influence within the watershed. The most important impact was caused by hydraulic mining for gold between 1852 and 1884 (Jaffe et al., 2007; Krone, 1979), resulting in an excessive and mercury-contaminated supply of sediments to the Bay. When hydraulic mining came to a halt, there was a considerable decline of sediment loads which was later enhanced during a period of Delta and watershed modifications from 1910 to 1975 (Barnard et al., 2013). This period included reservoir construction and Delta land reclamation projects, declining tidal marsh area and increasing flow conveyance through the Delta. The Bay's sediment trapping efficiency decreased with the decline of tidal marsh area, which had a considerable effect on the sediment balance (Atwater et al., 1979). Flow-regulating structures trapped sediment in their upstream and freshwater export facilities extracted sediment from the system (Kimmerer, 2004; Oltmann, 1996, 1999). This decrease in sediment load continued toward the end of the twentieth century while gradually leveling off and resulting in the current low SSC levels (Ganju et al., 2008; Wright & Schoellhamer, 2004).

During the hydraulic mining period, San Pablo Bay received a high sediment load which resulted in a net accretion of $256 \pm 14 \times 10^6$ m^3 from 1856 to 1887 and mudflats area increased (Jaffe et al., 2007). During the following period of decreasing sediment supply and Delta and watershed modifications, the mudflats became lower although they expanded laterally and narrowed the channel at the same time. In the mid-twentieth century, San Pablo Bay became net erosional (Jaffe et al., 2007; Kimmerer, 2004) and the sediment supply from local tributaries (Petaluma River and Sonoma Creek) became more important relative to the supply from the Sacramento and San Joaquin Rivers (Lewicki & McKee, 2010; McKee et al., 2013). Ganju et al. (2004) studied the sediment exchange between San Pablo Bay and its tributaries. Their analysis showed a tidally oscillating sediment mass which is effectively trapped within their confluence region except during the high flow conditions where a net seaward transport occurs.

SLR combined with the decreased fluvial sediment supply are posing new challenges to the system. Shallow mudflats might not be receiving the required sediment to cope with SLR causing their area to decline. If not for restoration projects, the sustainability of mudflats and adjacent tidal marshes will potentially be at stake (Barnard et al., 2013; Kimmerer, 2004). Because of their wave attenuating effect, drowning of marshes and mudflats will increase wave attack on existing levee systems. Thus, SLR poses a threat to the critical infrastructure around the Bay (Knowles, 2009). SLR also increases the risk of dike breaching within the Delta, which would alter hydrodynamics and sediment transport in the system.

It is unclear what SSC levels will be in the coming century. A better understanding of the physical mechanisms is needed in order to project the future sediment load (Wright & Schoellhamer, 2004). Also, climate change increases the uncertainty as it is expected to affect the future sediment yield. When performing a morphological forecast for Suisun Bay, Ganju and Schoellhamer (2010) applied a decreasing sediment supply by extending the declining trend identified by Wright and Schoellhamer (2004). This method yielded a 34% decrease in sediment supply for their 30-year modeling period. Modeling performed by Achete et al. (2017) showed that SLR is expected to increase the Delta's suspended sediment discharge due to an increased tidal action and its induced suspension. The combined effects of SLR and a drop in the sediment load resulted in a considerable decline of SSC levels in the Delta.

2.9. Regional SLR

Tidal gauge records from a location near the Golden Gate Bridge showed that during the period from 1855 to 1999, mean sea level (MSL) rose with a rate of approximately 1.5 mm/year (Flick et al., 2003; R. Smith, 2002). However, this rate has increased considerably over the past decades to more than 3 mm/year (R. Smith, 2002). NRC (2012) projections for the San Francisco area range from 43 to 167 cm with a median value of 91.9 cm by the end of the 21st century. They forecast a rise of 4–30 cm by 2030, 12–61 cm by 2050, and 43–167 cm by 2100 compared to 2000. In this research we implement three SLR scenarios by 2100 to cover the wide range

of uncertainties: (1) an optimistic scenario (42 cm); (2) an intermediate scenario (84 cm); and (3) a worst-case scenario (167 cm).

3. Modeling

Van der Wegen, Jaffe, and Roelvink (2011) and van der Wegen and Jaffe (2013) developed a model setup for hindcasting the 1856–1887 depositional period and the 1951–1983 erosional period in San Pablo Bay, respectively. They applied different river flow forcing and sediment supply to reflect decreasing sediment supply by the cease in hydraulic mining and dam construction as well as more regulated stream flows by increased conveyance and reservoir operations. In addition, van der Wegen and Jaffe (2013) applied a slightly modified wind field and sediment erosion to optimize model skill.

We implemented the same model setup and generally the same parameter settings as previous studies along with some minor modifications. The average grid size is about 550 × 550 m. The hydrodynamic time step is 2 min indicating that we include short time scale processes covering intratidal dynamics. The model is 3-D with 15 vertical sigma layers and includes saline-fresh water interaction while wind fields generate wave heights up to 0.3 m. In the sigma layer approach, number of layers is spatially constant and the top and bottom layers follow the water surface and bottom topography, respectively. Higher vertical grid resolution was implemented near the bed and water surface to provide adequate representation of the near-bed velocity shear and wind-wave action, respectively. To save computational time we use the morphological acceleration factor (MF; Roelvink, 2006) to model a representative single high-low river cycle instead of modeling 30 consecutive years each with a wet and dry season. We start with a 1 month of wet season with a MF of 30 followed by 4 months of dry season with a MF 82.5 which adds up to 30 morphological years. The wet season is assigned a lower MF to provide a better representation of the higher morphological activity that occurs during the wet season compared to the dry season. van der Wegen, Jaffe, and Roelvink (2011) and van der Wegen and Jaffe (2013) extensively tested this approach of separate scaling and the MF values implemented. With the use of the MF and the parallel computations option in D3D, the resulting model simulates 250 morphological years (≈3.5 hydrodynamic years) in about 8 days on a 4 core (2.6 GHz) computer. The supporting information provides a more detailed description of the model setup (Hoitink et al., 2003; Kuijper et al., 2004; Lesser, 2009; Partheniades, 1965; van der Wegen, Dastgheib, et al., 2011; van der Wegen, Jaffe, & Roelvink, 2011; Van Rijn et al., 2004; Winterwerp & Van Kesteren, 2004).

Our starting point is to model an entire ~250-year period with constant wind forcing conditions and sediment characteristics, while adapting only the river flow forcing and SSC at the landward boundaries and implementing a SLR at the seaward boundary. A single run consists of a 127-year hindcast period from 1856 to 1983 (used for validation while 1983 was the last bathymetric survey for the area) and a 120 years forecast from 1983 to 2103. We break down the modeling period into eight 30- to 34-year periods (Figure 2). The four periods during the hindcast period correspond with available bathymetric surveys (i.e., 1856–1887, 1887–1921, 1921–1951, and 1951–1983). The remaining four forecast periods are set to 30-year intervals (i.e., 1983–2013, 2013–2043, 2043–2073, and 2073–2103).

Figure 2 shows the modeling timeline while indicating the imposed boundary conditions for each period. For example, the river discharge imposed during the wet and dry seasons of the 1856–1887 period is 5,000 and 350 m^3/s, respectively. van der Wegen, Jaffe, and Roelvink (2011), and van der Wegen and Jaffe (2013) used the wet season river discharge as a calibration parameter leading to lower discharge during the erosional period (2,100 m^3/s in 1951–1983) than during depositional period (5,000 m^3/s in 1856–1887). Although we could not find clear indications on decreasing discharges over the past 150 years in literature, the different values may reflect somehow the change in river flow regime as the result of dam construction and conveyance measures in the catchment. In addition to the discharge decreasing trend, we imposed decreasing SSC at the boundary leading to an 1856–1983 decay in sediment load similar to values suggested by Ganju et al. (2008) and presented by Wright and Schoellhamer (2004).

The forecast from 1983 to 2103 is performed using the 1983 modeled bathymetry as an initial condition. During the forecast, the SSC is kept constant while the sea level starts rising starting from 2013 to 2103. This SLR is imposed at the seaward boundary of a large D3D FM model (see Text S3; Achete et al., 2015; Martyr-Koller et al., 2017; Vroom et al., 2017) that covers the entire San Francisco Bay-Delta system and is used to derive the hydrodynamic boundary conditions for the smaller D3D North Bay model used in this study.

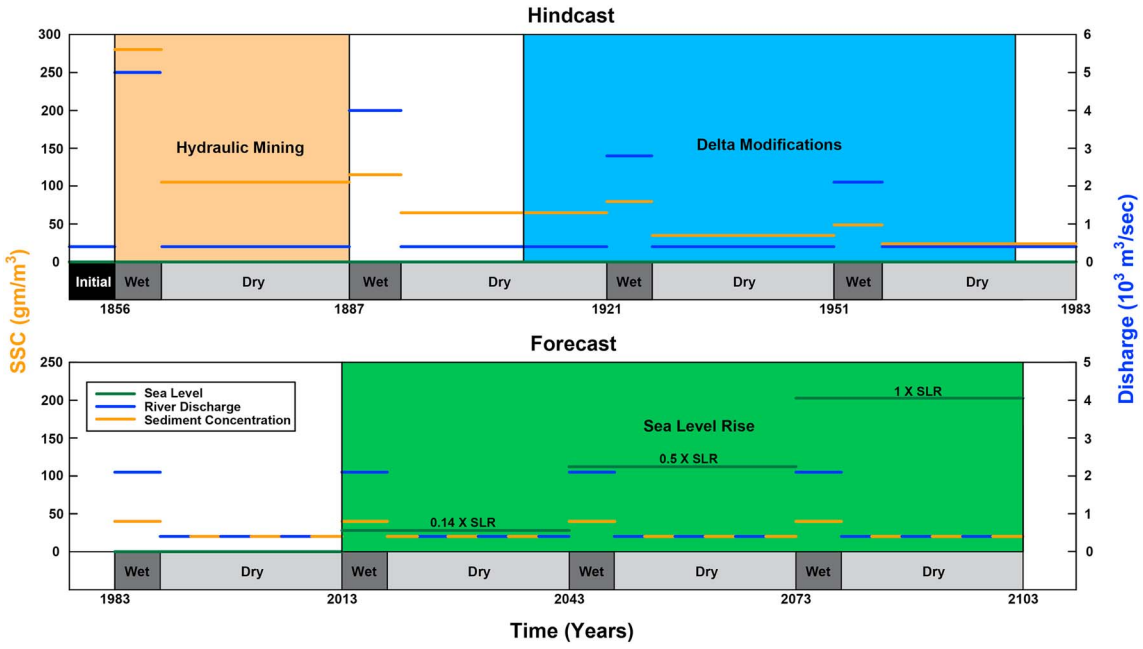

Figure 2. Schematization of the modeling timeline showing the hindcast (1856–1983) and forecast (1983–2103) along with the associated boundary conditions. The orange, blue and green lines represent the SSC, river discharge, and sea level, respectively. Sea level is increased for the forecast scenarios with 14%, 50%, and 100% of the total SLR imposed for 2013–2043, 2043–2073, and 2073–2103 periods, respectively. SLR = sea level rise.

Implementing this approach enables us to account for the SLR-induced variations in the tidal signal and river flow at the D3D North Bay model boundaries. SLR is imposed incrementally for each 30-year period with the magnitude of the rise calculated using a sine curve and the value at the end of each period. For example, a 167 cm SLR is imposed as 22, 84, and 167 cm for the 2013–2043, 2043–2073, and 2073–2103 periods, respectively.

4. Results

4.1. Hindcast

Comparing the 1856 initial bathymetry (Figure 3a) to the measured and modeled 1983 bathymetries (Figures 3b and 3c) shows that the model provides a good representation of the 127-year morphological development of the intertidal area (<0 MLLW), shoals (0–5 m MLLW), and channel (>5 m MLLW) during the hindcast period. This is also reflected by the good correspondence of observed and modeled cumulative sedimentation/erosion patterns (Figures 3e and 3f) and by a high Brier Skill Score of 0.54 (Excellent Category, see Table S2).

Both measurements and hindcasts show a significant increase in intertidal area caused by deposition at the Bay's margins. The model captures the considerable deposition volumes over the shoals near the main channel margin which resulted in a narrower main channel. The secondary channel fills in fully. Model results reflect the observed slightly erosional shoals to the west and the east of the secondary channel.

Figure 3d shows that the largest discrepancy exists near the main channel margin. The model hindcasts a total cumulative deposition of 3.48×10^8 m^3 which is about 20% larger than the observed 2.85×10^8 m^3. Compared to the 1983 measurements, the modeled channel is generally shallower along the model domain, wider in the west (Figure 3g), and narrower in the east (Figure 3h). A possible explanation is that the applied sand fraction in the deep section of the channel is coarser than in the reality. Also, in the model, we do not simulate (limited) dredging activities in the channel (Jaffe et al., 2007).

The model reflects the observed depositional trend in periods from 1856 to 1951 and a slightly erosional trend from 1951 to 1983 (Figure 4). Both measurements and hindcasts show erosion in the deepest channel section during all periods. The model slightly underestimates this erosion, especially during the 1887–1951 period. Hindcasts show deposition at the northern channel bank which starts from the eastern end and

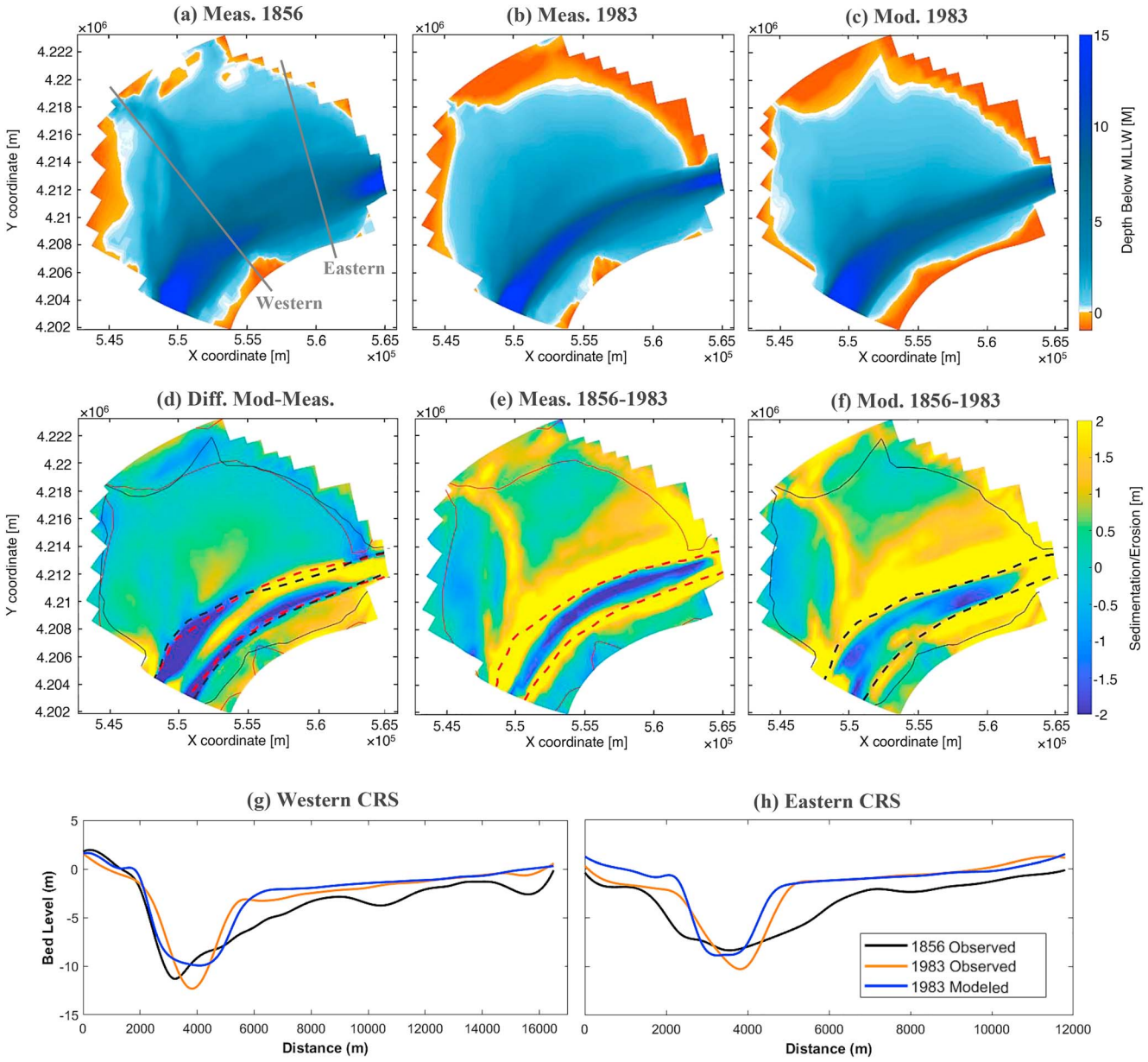

Figure 3. Top panel shows San Pablo Bay bathymetry (a) 1856 measured, (b) 1983 measured, and (c) 1983 modeled. Middle panel shows (d) difference between 1983 measured and modeled bathymetries, (e) measured, and (f) modeled cumulative sedimentation/erosion from 1856 to 1983. Continuous and dashed lines represent the 0 and 5 m MLLW contour lines, respectively. The observed 1983 contours are shown in red in both (d) and (e). Bottom panels are (g) western and (h) eastern bed level cross-sections (CRS) shown in (a).

propagates gradually with time toward the western end. This behavior is observed in measurements, however, the deposition at the eastern end starts earlier in hindcasts (1887–1921) than that in observations (1921–1951). For the southern channel bank, hindcasts match the measured trend of considerable deposition during the 1856–1887 period.

Figures 5a–5c show that the model reproduces changes in channel, shoal, and intertidal area. Channel narrowing occurs throughout the entire hindcast with a gradually decreasing rate over time (Figure 5a). The model provides a good representation of this trend showing higher rates in the wet season than that for the dry season which implies that its main driver is bank deposition associated with the wet season sediment pulse. This is especially evident for the eastern side during the 1856–1887 wet season. Shoal area remains fairly constant over time (Figure 5b) due to the fact that it lies between a narrowing channel and

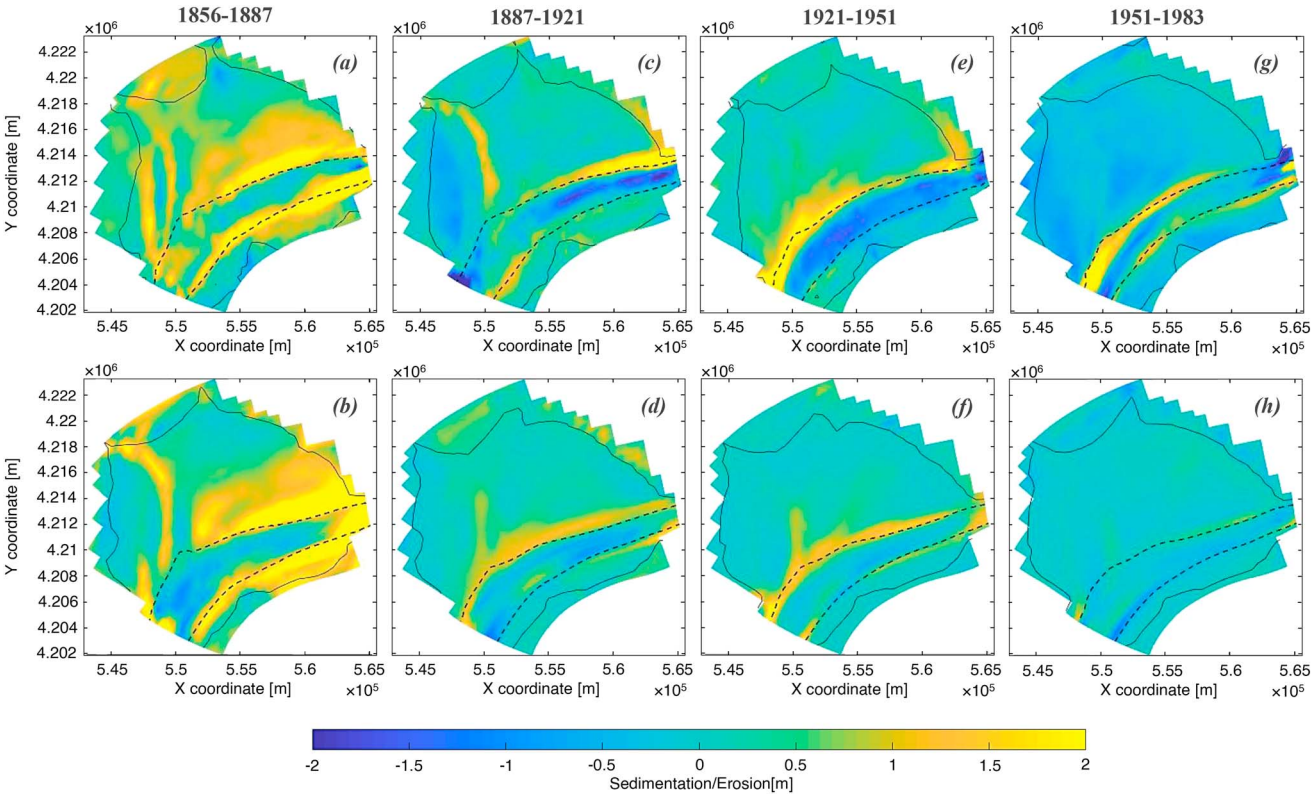

Figure 4. Measured (top panel) and modeled (bottom panel) sedimentation/erosion maps for each period.

widening intertidal flats. Channel banks experienced sedimentation and shifted to shoals at the same time deposition landward transformed shoals into intertidal flats.

Hindcasts successfully capture the large increase in intertidal area that occurred during the depositional period from 1856 to 1951 (Figure 5c). Unlike the channel narrowing, this intertidal area growth occurs during both the wet and dry season with the latter having the higher contribution. A possible explanation is that a portion of the sediment deposits during the wet season sediment pulse while a larger portion is supplied by wave-induced resuspension during the dry season from either newly deposited wet season sediment during or older sediment being eroded from the shoals. Intertidal flats accretion is highest during the 1856–1887 period and continues with a gradually decreasing rate toward the end of the depositional period (1951), while model results underestimate the drop in intertidal areas after 1951.

Investigating the development of the BSS (Brier Skill Score; Bosboom et al., 2014; Bosboom & Reniers, 2014; de Alegria-Arzaburu et al., 2011; Sutherland et al., 2004; Text S7) and its Murphy and Epstein (1989) decomposition over time (Figure 5d) provides a more objective insight into model performance. For the depositional period from 1856 to 1887, the model shows good performance (BSS of 0.47). The low mean error ($\gamma = 1.8 \times 10^{-3}$) indicates good skill in hindcasting the total depositional volume. The model hindcasts a total depositional volume of 2.46×10^8 m^3 which is about 3% higher than the 2.39×10^8 m^3 observed during this period.

The model performance gradually increases to a BSS of 0.63 in 1951, (1) α increased (0.36 to 0.52) indicating a phase error decrease; (2) β decreased (0.38 to 0.15) illustrating a better performance in hindcasting the sedimentation/erosion amplitudes/phases; (3) γ increased (1.8×10^{-3} to 1.1×10^{-2}) showing a decreased performance in mean level; and (4) ε decreased (0.96 to 0.80). The small decrease in BSS after 1951 is attributed to the small net erosion being more difficult to model than the large depositional signal (van der Wegen & Jaffe, 2013). The shoal erosion is underestimated during the 1951–1983 period. Another reason is that the ε value dropped sharply from 0.80 to 0.43. However, it is important to note that a decreasing epsilon value does not directly indicate a decreased model performance instead it indicates that the difference between the

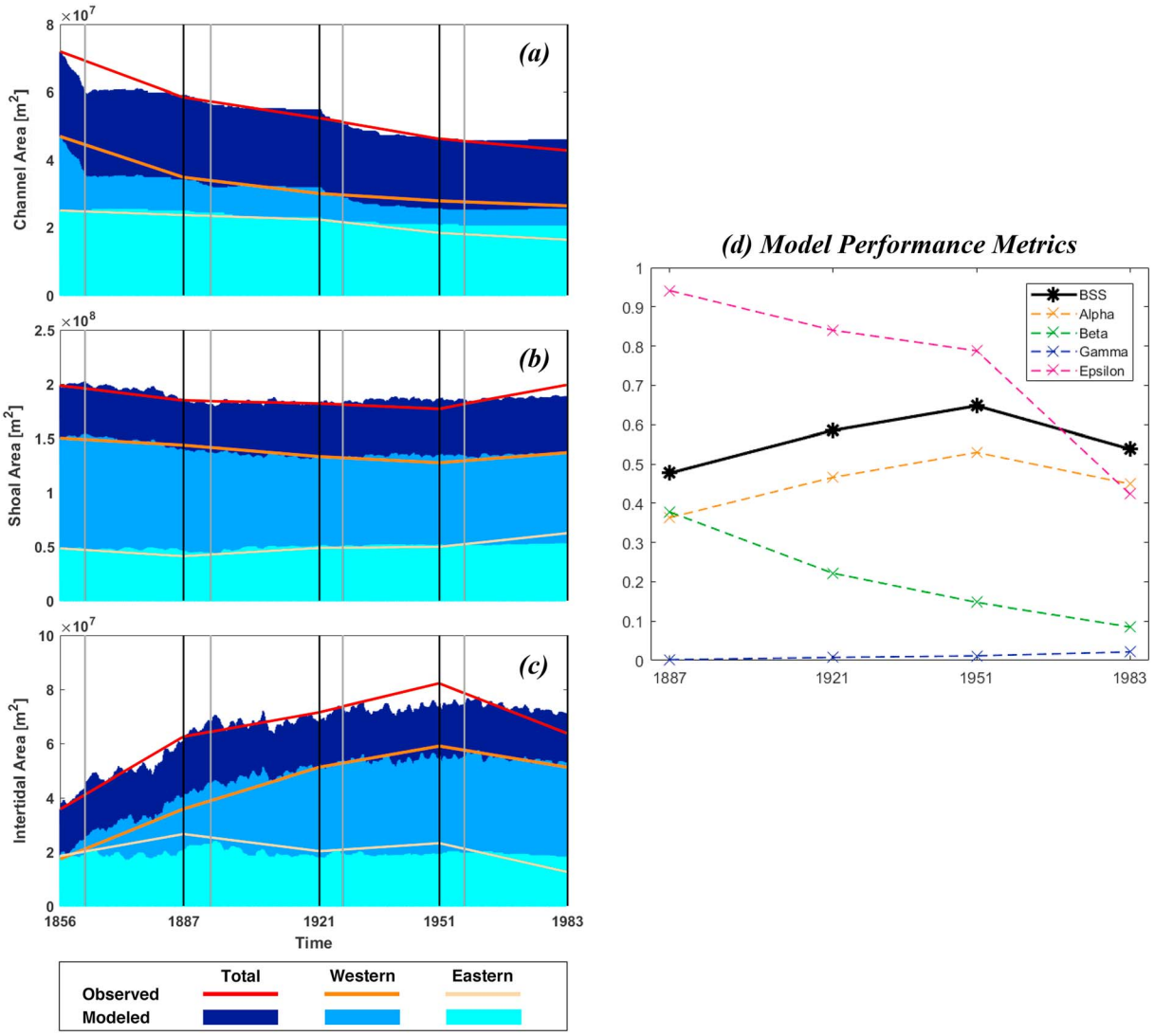

Figure 5. Modeled (color shaded) and observed (lines) spatial coverage of the model domain and its changes over time divided between (a) channel (< -5 m MLLW), (b) shoals (0 to -5 m MLLW), and (c) intertidal area (>0 m MLLW) for both the eastern and western sides of San Pablo Bay. Vertical gray lines indicate the end of the wet season runs. Right panel (d) shows the development of the BSS score and its Murphy and Epstein (1989) decomposition throughout the hindcast period compared to the 1856 initial bathymetry.

1856 initial reference bathymetry and the compared bathymetry have dropped, hence errors are more severely penalized. A sensitivity analysis was carried out for the hindcast period and the results for some selected sensitivity runs are presented in section 5.2.

4.2. Forecast

We performed a morphological forecast that extends 120 years from 1983 till 2103 for a No SLR scenario along with three SLR scenarios of a 42 (optimistic), 84 (intermediate), and 167 cm (worst-case) rise during the final approximately 100 years (Figure 6). Forecasts show that for the No SLR scenario, the Bay's erosional trend continues till the end of the 21st century (Figures 6a and 7a). By 2103, the spatially averaged intertidal area height decreases by 12.8 cm while an average shoal erosion of 4.1 cm occurs (Table 1). The main drivers of this erosion are the lack of sediment supply from the Delta and the wind-wave attack. Also, channel slope deposition continues resulting in a narrower and deeper main channel. However, the average channel depth remains relatively constant (+2.0 cm) as the deposition and erosional volumes are in the same order of magnitude.

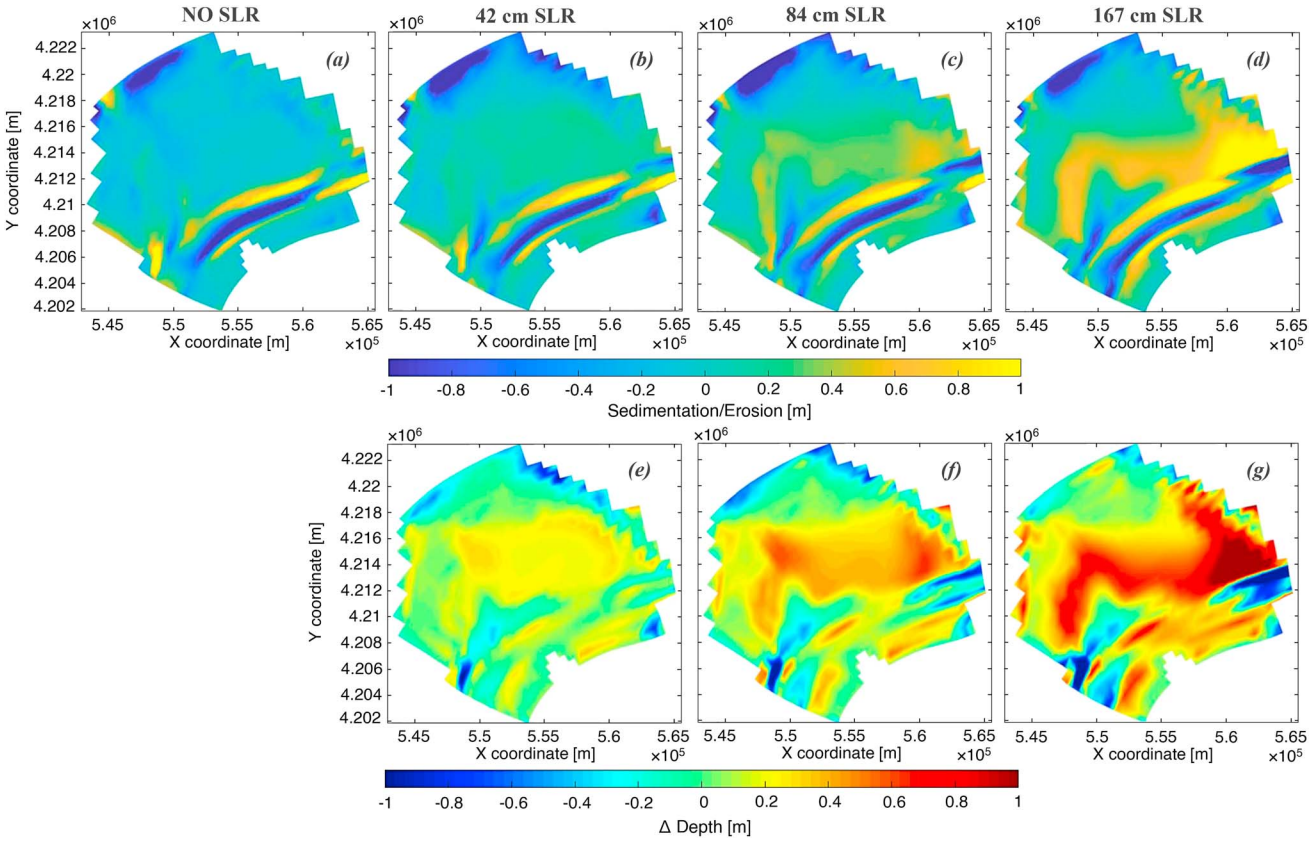

Figure 6. Top panel shows the cumulative sedimentation/erosion maps from 1983 to 2103 for the (a) no SLR and (b, c, and d) SLR scenarios. Bottom panel shows SLR-induced bed level changes for the (e) 42, (f) 84, and (g) 167 cm SLR scenarios. For example, (f) is the difference between (c) and (a) with the red and blue colors indicating higher and lower bed levels, respectively. SLR = sea level rise.

During the hindcast period, our simulations slightly overestimate the cumulative deposition volumes (Figure 7a). However, simulations are still able to capture the shift from a depositional Bay (1856–1951) to an erosional Bay (1951–1983). The forecast shows the continuation of this erosion from 1983 to 2013 and, for the No SLR scenario, a net erosion of about 20×10^6 m^3 from 2013 to 2103. In contrast, for the 42 cm SLR scenario the Bay is neither strongly erosional nor depositional. However, for the 84 and 167 cm scenarios, the Bay turns from erosional to depositional with net deposition of 16×10^6 and 58×10^6 m^3, respectively. The patterns of deposition and erosion are similar for all three scenarios, the deposition magnitude increases with higher SLR (Figures 6s–6g).

Shoals experience a net depositional trend for the three SLR scenarios. This trend is due to an increased sediment trapping efficiency, deposition is mainly driven by the SLR-induced increase in water depth which decreases the effect of waves on the bottom and creates calmer flow conditions that enhance mud deposition. This deposition is highest near the channel and decreases gradually toward the landward margins. In response to SLR, the average shoal depth increased by 12.3, 23.7, and 40.4 cm for the 42, 84, and 167 cm SLR scenarios, respectively. However, this accretion rate is only 25–30% of the SLR rate which means that it cannot keep up with the rising sea levels and the relative shoal depth will increase leading to the drowning of San Pablo Bay shoals.

Model results (Figure 7b) show an increase in intertidal area during the depositional period (1856–1953). Following that, they begin decreasing gradually toward the present-day resulting in an intertidal area of 6.91×10^7 m^2 in 2013. For the No SLR scenario, this gradually decreasing trend is predicted to continue with a relatively constant rate which would lead to the loss of approximately 13% of the current (2013) intertidal area by the end of the 21st century. Implementing the different SLR scenarios showed a sharp drop in intertidal area and a considerable loss of about 43%, 66%, and 91% of intertidal area by 2103 for the 42, 84, and 167 cm SLR scenarios, respectively.

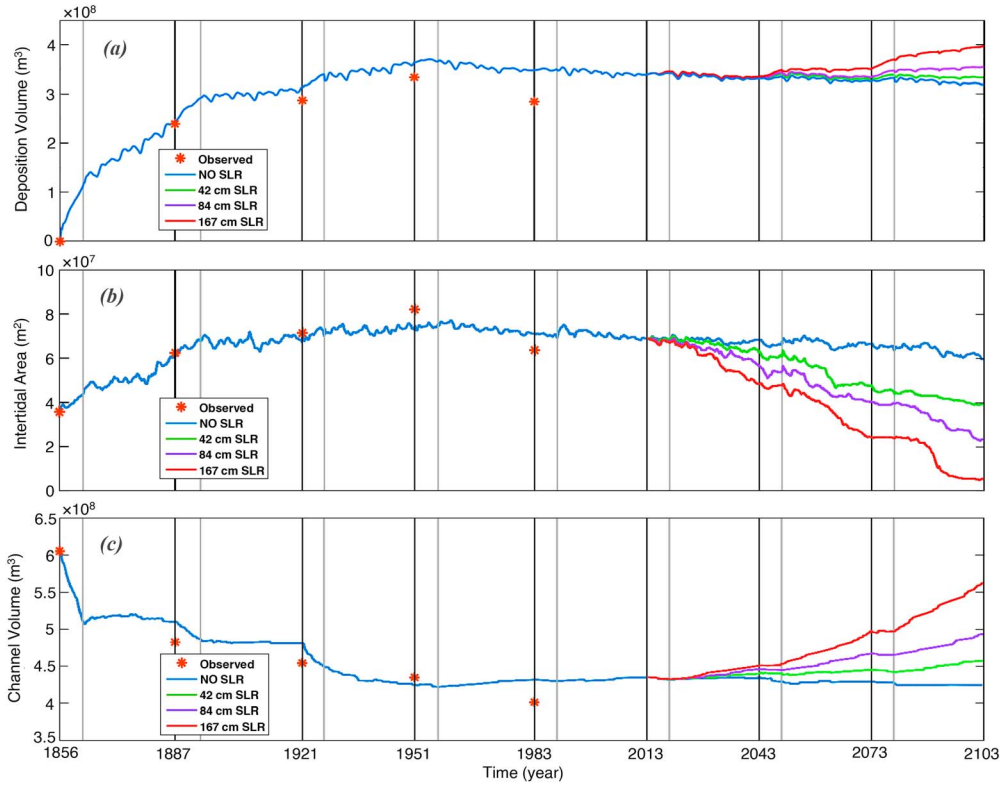

Figure 7. Quarter millennium development of (a) depositional volumes, (b) intertidal area, and (c) channel volume for the no SLR (blue) and the 42 (green), 84 (purple), and 167 cm (red) SLR scenarios. SLR = sea level rise.

In addition to the inundation-induced loss of intertidal area, SLR increases the landward extent of wind-wave attack which enhances erosion along the landward margins. For the optimistic 42 cm SLR scenario, this effect results in a spatially averaged intertidal area erosion of 15.2 cm. While, for the worst-case 167 cm SLR scenario, this erosion is observed at the early stages but as the inundation height increases, the wave-induced bottom shear stress starts dropping causing the erosional trend to shift to depositional. However, the average depositional magnitude (+7.1 cm) is much less than the rising sea level (167 cm), eventually leading to inundation-induced loss of intertidal area.

Channel bank deposition and erosion in the channel observed for the different SLR scenarios (Figures 6b–6d) are similar to the No SLR scenario (Figure 6a). However, Figures 6e–6g show that SLR caused slightly higher bed levels in the middle section and lower bed levels toward the eastern and western end of the main channel. This trend is most clear for the 167 cm scenario (Figure 6g), especially at the eastern channel end where the elevation difference is more pronounced, even reaching more than 1 m compared to the No SLR scenario. The eastern channel erosion starts from Carquinez Strait (not shown) which experienced considerable deepening due to SLR. This eroded sandy sediment is carried seaward and settles in the shallower and calmer

Table 1
Spatially Averaged Bed Level Changes Between 1983 and 2103 for the No SLR and for the Three SLR Scenarios Relative to the No SLR Case

			Δ depth relative to no SLR (cm)		
Depth range (MLLW)	Coverage area (%)	No SLR (cm)	+42 cm SLR	+84 cm SLR	+167 cm SLR
>0 m (Intertidal)	24.2	−12.8	−15.2	−13.1	+7.1
0 to −5 m (Shoals)	60.7	−4.1	+12.3	+23.7	+40.4
<−5 m (Channel)	15.1	+2.0	+1.1	−4.1	−6.6

Note. SLR = sea level rise.

middle section of San Pablo Bay channel eventually resulting in higher bed levels. This behavior also occurs in the western end at San Pablo Bay Strait; however, the sediment eroded there gets carried seaward out of the model domain.

Throughout the hindcast period, the channel volume decreased significantly (Figure 7c). Forecasts show that, without SLR, the channel volume will experience a slight drop toward the end of the 21st century and imposing SLR results in a notable increase in channel volume. This increase occurs during the dry season, while during the wet season it is either constant or there is a slight drop. This is caused by the wet season sediment pulse that enhances channel bank deposition which is in the same order as the SLR-induced added water volume.

5. Discussion

5.1. General Model Performance

The high model skill obtained in this work is in line with model skill reported by Dam et al. (2016) when performing a 110-year morphological hindcast (1860–1970) for the Western Scheldt Estuary in the Netherlands with a similar process-based model. They observed a decreasing skill in the first decades and an increasing skill to a value of 0.52 after 110 years. A possible explanation for this behavior is a decadal morphological spin-up time in which the bathymetry adjusts to its roughly schematized model parameters, imposed constant forcing conditions, and process descriptions (Dam et al., 2016). Afterward, the model captures the morphological development that is governed on the long-term by the interaction of the major tide with the estuary's plan form. We think that the interaction between major tidal and fluvial forcing and the estuary's plan form also play a major role in San Pablo Bay morphodynamic development. Another explanation is that the sediment supply signal is very strong in the first decades and dominates more subtle processes such as wave action. Van der Wegen and Jaffe (2013) showed that net volume changes during the erosional period are an order of magnitude smaller than the depositional period. The wave-driven erosion is subtle compared to the sediment supply signal during the preceding decades and leads to lower skill scores than during the depositional period.

5.2. Hindcast Sensitivity

We performed a sensitivity analysis for the base case hindcast presented in section 4.1 to achieve optimal skill and a better understanding of the processes that govern the morphological development of San Pablo Bay. In this section, we present a selected set of sensitivity runs: (1) excluding salinity effect (No Salinity); (2) excluding 3-D processes (2DH-Model); (3) excluding wind-wave generation (No Waves); and (4) imposing SLR in the hindcast (Hindcast SLR).

5.2.1. No Salinity

Salinity exclusion affects several aspects, most importantly it eliminates salinity stratification and density currents. Two-layer flow and gravitational circulation associated with salinity gradients have been noted in previous studies to have a considerable effect on North Bay sediment dynamics (e.g., Elmilady, 2016; Ganju & Schoellhamer, 2008). Our model results (Figures 8a and 8e) confirm the importance of salinity-driven processes on the long-term morphological development of San Pablo Bay. Excluding salinity results in considerably lower bed levels at the estuarine margins, shoals, and channel banks. Channel narrowing and shoal accretion are very poorly represented. This can be explained by shoal accretion first starting with channel bank deposition that gradually propagates landward toward the estuarine margins (e.g., van der Wegen et al., 2016).

Despite a slight increase in sediment import from its landward boundary, San Pablo Bay's net depositional volume for the No Salinity scenario (1.44×10^8 m^3) was significantly lower than that for the base case simulation (3.48×10^8 m^3) and measurements (2.85×10^8 m^3). This was caused by a simultaneous significant increase in the seaward sediment export from San Pablo Bay, resulting in a decrease of the Bay's sediment trapping efficiency (Import/Export). This can be explained by salinity stratification, landward directed density currents, and gravitational circulation increasing sediment retention in the system. This occurs primarily because of the resulting calmer conditions near the bottom that enhance sediment settling and drives landward directed sediment transport (Elmilady, 2016).

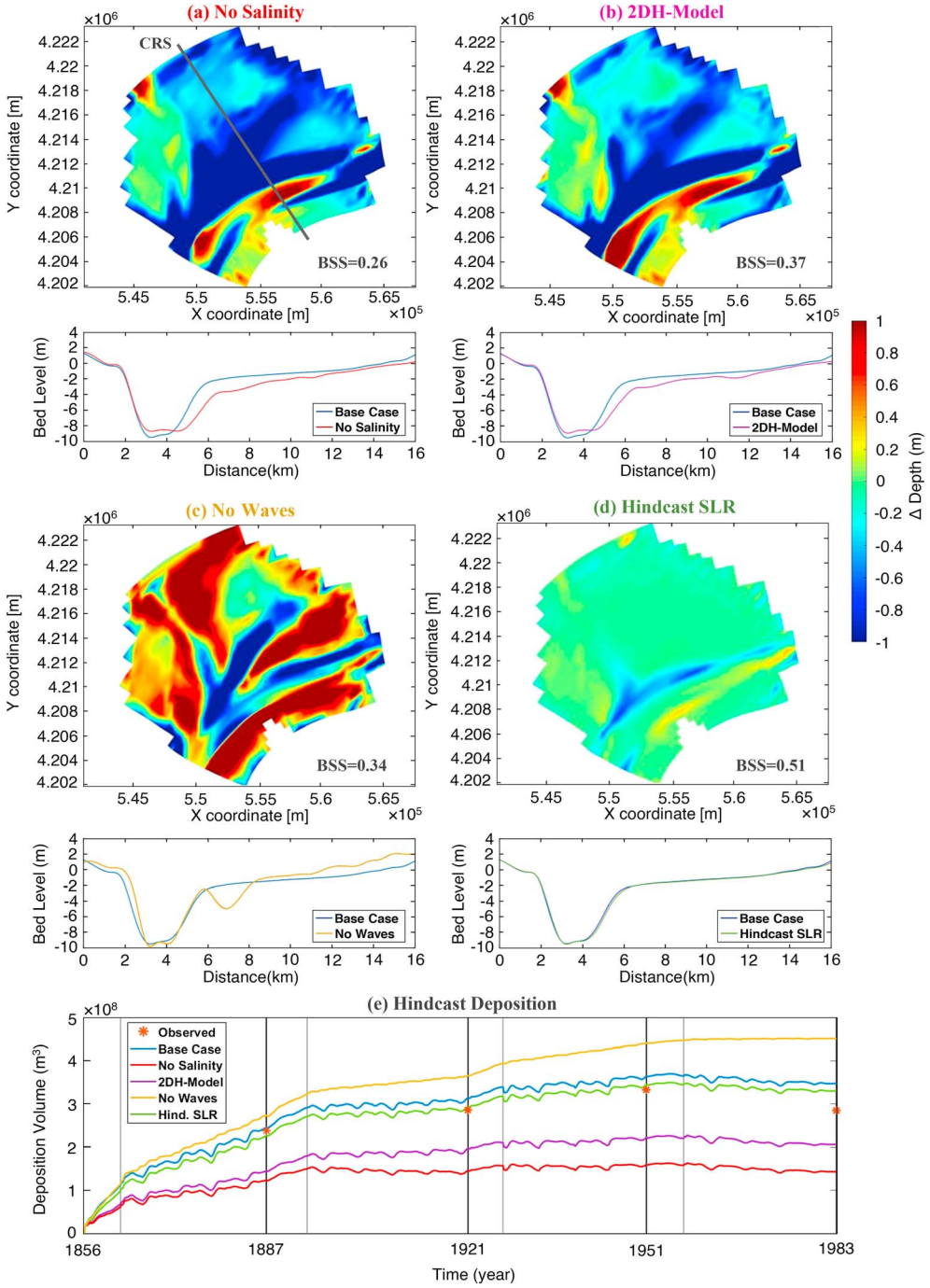

Figure 8. Hindcast sensitivity results for (a) no salinity, (b) 2DH-model, (c) no waves, and (d) Hindcast SLR. Maps indicate bed level difference between sensitivity run and base case, red and blue color donates higher and lower than base case bed level, respectively. Transects below each map are bed level cross-sections along CRS shown in (a) for base case (blue) and sensitivity run. Bottom panel (e) shows deposition volumes for the hindcast period. SLR = sea level rise.

5.2.2. 2DH-Model

Running the model in a 2DH form instead of the 15 sigma layers (Figure 8b) showed a high resemblance with the No Salinity sensitivity run (Figure 8a). This suggests that salinity-driven 3-D processes have considerable influence relative to other 3-D processes.

Similar to the No Salinity case, there was a slight increase in sediment import from the Delta along with a considerable simultaneous increase in the seaward sediment export from the Bay. This resulted in a net depositional volume for 2DH-Model (2.03×10^8 m^3) that is considerably lower than the base case (3.48×10^8 m^3). However, the sediment trapping efficiency for the 2DH model was slightly higher than that for the No Salinity case that is reflected in a 41% increase in deposition volumes. A possible explanation for this increase is that despite neglecting the effect of the salinity stratification and gravitational circulation, the 2DH model still simulates the landward directed density currents driven by the longitudinal salinity gradient between San Pablo Bay and Suisun Bay.

5.2.3. No Waves

The sediment input from the Delta is almost the same as the base case, however, the seaward sediment export decreased, hence resulting in a more depositional San Pablo Bay. This increase in sediment trapping efficiency was caused by a 26% drop in bed shear stresses over the shoals. This drop resulted in a net deposition of 4.46×10^8 m^3 which is about 35% higher than that for the base case. Most of this difference occurred during the dry season when wind-waves play an important role in sediment resuspension and redistribution. Also, by inspecting Figure 8e and comparing the No Waves run with other simulations, we found that wind-waves are responsible for the—erosive—signal fluctuations that mainly occur during the dry season throughout the hindcast.

Compared to the base case (Figure 8c), significantly higher depositional volumes occur on the landward margins and their adjacent shoals resulting in a significant increase of intertidal area and higher elevation shoals. The decreased flow over the accreting shoals resulted in larger flow volumes through the main channel which enhanced its erosion and caused the formation of a secondary channel that bisects the north-eastern shoals.

The No Wave simulation clearly illustrates that wind-waves play a very important role in maintaining the channel-shoal structure in San Pablo Bay by limiting shoal elevation and ensuring a gradual transition in elevation based on wave energy.

5.2.4. Hindcast SLR

Between 1855 and 1999, the MSL at the Golden Gate rose with a rate of approximately 1.5 mm/year (Flick et al., 2003; R. Smith, 2002). This rate equates to approximately 19 cm SLR during the modeled hindcast period. Our model results (Figure 8d) show that implementing this gradual SLR during the hindcast has a minor impact on the morphological development. Less deposition occurred on the main channel northern bank that resulted in a slight decrease in overall depositional volumes to 3.28×10^8 m^3, which is closer to observed volumes than the base case (Figure 8c). The end BSS decreased slightly to 0.52, but still remained on the same order as that for the base case (0.54). Also, when modeling the morphological development of San Pablo Bay during the erosional period, van der Wegen and Jaffe (2014) applied a 20-cm rise/drop in MSL and their results showed that it had a minimal effect on the erosional/deposition patterns and volumes, eventually concluding that it is only when SLR accelerates that larger influences are expected. Furthermore, Rossington and Spearman (2009) showed that the 2 mm/year SLR observed over the past 100 years in the Thames Estuary (UK) had a limited effect on the morphological development of the estuary compared to the anthropogenic influence and the predicted future SLR.

Based on the above, the effect of this 1.5 mm/year rise was excluded in our base case. This exclusion enables us to create a hypothetical base case NO SLR scenario that extends into the forecast that allows us to isolate the effect of future SLR by acting as a comparison point for the other three SLR scenarios. Errors resulting from this assumption are small compared to implementing SLR in the hindcast and then abruptly stopping it in the forecast. Van der Wegen et al. (2016) showed that the adaptation time scales of mudflats for abruptly changing boundary conditions can be on the order of decades. Also, our simulations following 2103 (not shown) indicated that when SLR is abruptly stopped, the system will still be adapting for decades. The exclusion of SLR in hindcasts serves the main aim of this study, which is to understand the effect of the predicted accelerated SLR on the morphological development.

5.3. Forecast Analysis

SLR increases San Pablo Bay's sediment trapping efficiency and shifts the system's erosional trend to a depositional one for the intermediate (84 cm) and worst-case (167 cm) SLR scenarios. This increase in deposition is mainly driven by the increase in mean water depth which under similar wind-wave conditions results

in a decreased effect of waves on the bottom and creates conditions that enhances mud deposition, especially on the shoals. As a result, the shoals capture more sediment and start accreting in response to SLR. However, due to the low sediment supply from the Delta, the accretion rate is only between 25% and 30% of the SLR rate and San Pablo Bay shoals are drowning. For a similar depth range, Ganju and Schoellhamer (2010) indicated that Suisun Bay shoals are expected to accrete at a rate between 35% and 40% of the SLR. This higher value can be explained by Suisun Bay being located closer to the inland source of sediment supply.

In San Pablo Bay, the rate of shoal accretion is about 29%, 28%, and 25% of the SLR rate for the 42, 84, and 167 cm SLR scenarios, respectively. This relatively small variation between the different scenarios suggests the relative independence of accretion rates on the magnitude of SLR. Sediment supply sensitivity runs (not shown) illustrated that this rate is mainly dependent on the sediment load from the Delta. The current sediment supply is too low for the shoals to keep up with SLR. In addition, Figure 7a shows that the effect of SLR on the deposition volumes is small compared to the effect of the hydraulic mining period that delivered a huge sediment pulse to San Pablo Bay. This suggests that sediment supply from the Delta plays an important role in determining whether there is net erosion/accretion of the Bay.

Our forecasts showed that the current trend of channel narrowing and deepening will continue in the future at a gradually decreasing rate irregardless of SLR. However, we found that SLR enhances channel slope deposition leading to a narrower main channel at the eastern side of the Bay. In addition, forecasts showed considerable SLR-induced erosion starting in Carquinez Strait and propagating seaward toward the San Pablo Bay channel. We attribute this to the larger tidal prism conveyed to Carquinez Strait. For the worst-case 167 cm SLR scenario, this erosional trend can be clearly observed at the eastern side of the Bay. Additional simulations beyond 2103 showed that this erosion progresses gradually seaward leading to a deeper San Pablo Bay channel. This illustrates that at the end of the 21st century the system is still reacting to the imposed SLR and that the channel is expected to get deeper over time with a seaward residual transport. It might take decades, or even longer, for the full effect of this imposed SLR to change the morphology. The deeper channel sections like Carquinez and San Pablo Straits react faster to SLR than the shallower channel sections. A similar trend was forecasted by Ganju and Schoellhamer (2010) who showed that SLR results in deeper Suisun Bay channels. They found that the highest erosion occurred in the deepest sections of the channel from 18 to 20 m and decreases gradually and shifted toward being depositional for the 10–12 m depth range.

We identified a considerable threat to intertidal area. Model results showed that the 2013 intertidal area will experience a drop of 13%, 43%, 66%, and 91% by the end of the 21st century for the No SLR, 42, 84, and 167 cm SLR scenarios, respectively. The forecasted decrease for the No SLR scenario is mainly driven by the lack of sediment supply and the wind-wave attack which extended the Bay's erosive trend observed in the hindcast. Imposing SLR increased the intertidal area decline due to inundation and the increase of the landward extent of wind-wave attack, with the former having a higher contribution. When modeling the evolution of the South Bay mudflats to the end of the 21st century, van der Wegen et al. (2016) reported a decline of about 40% of intertidal area for the 167 cm scenario and a complete loss of intertidal area when combined with a 50% decrease in sediment supply.

Rising sea level will increase the inundation frequency of the intertidal mudflats, hence subjecting them to an increased wind-wave attack. For the 42 and 84 cm SLR scenarios, this resulted in erosive estuarine margins due to the lack of sediment supply to compensate for the increased wave attack. Ganju and Schoellhamer (2010) reported a similar trend of SLR-induced erosional estuarine margins in Suisun Bay. For the 167 cm SLR scenario, the large inundation height leads to a drop in the wave-induced bottom shear stresses and shifted this erosional trend to a depositional trend. However, the deposition rate was minimal compared to the SLR rate resulting in a considerable loss of intertidal area due to inundation.

Erosion, or accretion with a rate less than the SLR, resulted in inundation due to an increased relative water depth. This increase caused a transition in states where shoals turned to channel and intertidal mudflats turned to shoals. Consequently, salt marshes are expected to give way to the migration of their adjacent intertidal area. However, in this research, no accommodation space was implemented, thus intertidal area migration is not possible as the Bay's boundary was imposed as a fixed boundary. Migration will only occur in the case of no obstructions and accommodation space available (Kraft et al., 1992). In reality, there are no

obstructions and accommodation space is available at some locations in northern San Pablo Bay. At most locations in San Pablo Bay, however, migration is not possible due to obstructions.

The fate of San Pablo Bay salt marshes under SLR has been assessed in previous studies (e.g., Takekawa et al., 2013). At some locations, salt marshes are expected to be able to trap sediment eroded from mudflats and accrete with a rate that matches the SLR rate. At other locations, especially the young salt marshes, the SLR-induced increased inundation frequency is expected to drown salt marshes and give away for intertidal mudflat migration. The fate of San Pablo Bay intertidal mudflats heavily depends on whether or not salt marshes will give way for migration. The results presented in this research assume that migration is not possible, thus it can be argued it is a worst-case scenario. Indeed, we anticipate that the significant forecasted loss of intertidal mudflats would have been much lower if migration was possible. However, in this case, migration means the loss of valuable salt marshes.

5.4. Modeling Approach

There were some challenges associated with the forcing schematization. We imposed SLR in steps instead of a gradual rise. A gradual SLR would have resulted in a lower rise during the wet season than that for the dry season, while a sudden rise overestimates the SLR impact. However, comparing the results of both methodologies showed similar morphological behavior with a negligible difference in the magnitude of the deposition/erosion volumes that would not affect the conclusions. The reason is that a model spin-up exists when a new sea level is imposed.

We start the modeling with a wet season followed by a dry season. The order of seasons is of significance when considering a single 30-year period, especially for the hydraulic mining period. However, on the longer run the effect gradually becomes insignificant since it is overruled by the long-term morphological development.

5.5. Application to Other Estuaries

In this research, San Pablo Bay is presented as a case study. The value of this research extends beyond achieving a better understanding of SLR impact on the long-term morphological development of a particular system. Findings and the process-based methodology can be applied to estuaries with similar forcing conditions. In this estuary with low sediment supply and artificially regulated flows, we show that SLR poses a considerable threat to the estuarine environment. This situation is common in estuaries worldwide where the construction of flow-regulating structures upstream resulted in a considerable decline in the sediment supply and controlled discharges during the wet season significantly reduced the system dynamics. Not being able to accrete at a rate equal to or greater than the SLR rate will lead to the system drowning and the potential loss of valuable habitat. Landward migration is critical for the sustainability of those ecosystems. However, as is the case in San Pablo Bay, several estuaries around the world lack accommodation space due to urbanization pressure.

We illustrate the potential of applying the process-based modeling approach to identify governing processes and to simulate the morphological development over a centennial time scale. Such models can be a useful tool to assess the impact of climate change-induced perturbations on the morphological development of estuaries worldwide. In addition, we present and test a framework for performing such long-term morphological forecasts.

5.6. Future Research and Recommendations

We recommend further developments to this research such as using the developed model to assess the impact of SLR combined with other climate change-induced changes in sediment supply, river flow, and meteorological conditions. Moreover, there is value in including more processes (e.g., flocculation), specifying more detailed forcing description (e.g., wind conditions including extreme events), and incorporating the available accommodation space and surrounding salt marshes in the model. In addition, obtaining a more recent bathymetry would allow further evaluation of the model and investigation of Bay's erosional trend continuity. Also, investigating the impact of possible Delta polders breach on the upstream boundaries. Finally, studying the system on a longer time scale beyond the end of the 21st century could improve the understanding of estuarine evolution.

6. Conclusions

San Pablo Bay historical bathymetric surveys showed considerable morphological development from 1856 to 1983 due to variations in fluvial sediment load and discharges associated with a period of hydraulic mining for gold, modification of the Delta, and damming in the watershed.

Our 3-D processes-based modeling effort resulted in a reasonable reproduction of the morphological development that occurred during this period. Further extending our model simulations in a forecast to the end of the 21st century allowed us to study the effect of SLR on the Bay's morphological evolution. We identified that SLR poses a considerable threat to intertidal area when landward migration is not possible. SLR enhances the recent erosional trend due to the inability of the low sediment supply to compensate for the increased landward extent of wind-waves attack and inundation frequency.

Forecasts showed that SLR increases the Bay's trapping efficiency which for the intermediate and worst-case SLR scenarios caused the system to shift from being erosional to depositional. Despite that, San Pablo Bay drowns under all SLR scenarios. The decreased effect of waves on the bottom allows shoals to accrete in response to SLR. However, due to the low fluvial sediment supply, accretion is only 25–30% of the SLR and results in an increase in relative water depth.

Model results indicated that the behavior of main channel narrowing and deepening observed during the hindcast will continue to the end of the 21st century at a decreased rate and that it is not primarily SLR-induced. SLR enhances channel erosion which starts in the deepest channel sections with a seaward residual transport. By the end of the forecast, the system was still reacting to the imposed SLR.

The performed hindcast sensitivity analysis highlighted the considerable influence of the salinity-driven and 3-D processes on the long-term morphological evolution of the Bay. They decrease the seaward sediment export from the system resulting in a higher trapping efficiency. Wind-generated waves also play a very important role in sediment redistribution, limiting shoal elevation, and maintaining the channel-shoal structure.

Finally, our modeling exercise shows that process-based models can be a useful tool to achieve a better understanding of the morphodynamic response of estuaries to climate change-induced forcing conditions perturbations. Similar to the findings of Dam et al. (2016), we conclude that even with a large number of schematizations implemented, such models can perform well in estuarine environments, especially when considering centennial time scales.

Acknowledgments

This research is supported by the U.S. Geological Survey Priority Ecosystem Science and Coastal and Marine Geology Programs and the California Delta Science Program. This research is a part of the CASCaDE climate change project (CASCaDE contribution number 80). The authors thank all involved personnel for their support. The computational resources provided by SURFsara facilitated the modeling process. The authors highly appreciate the thoughtful comments by the three anonymous reviewers which helped improve the manuscript. The authors acknowledge Richard Marijnissen for his work that laid the foundation for this research. There is no restriction on the data used in this study, readers can download the historic bathymetries (Jaffe et al., 2007) from https://sfbay.wr.usgs.gov/sediment/sfbay/index.html and the numerical model configuration and results from 10.6084/m9.figshare.7392404.

References

Achete, F., van der Wegen, M., Roelvink, J. A., & Jaffe, B. (2017). How can climate change and engineered water conveyance affect sediment dynamics in the San Francisco Bay-Delta system? *Climatic Change*, *142*(3–4), 375–389. https://doi.org/10.1007/s10584-017-1954-8

Achete, F. M., van der Wegen, M., Roelvink, D., & Jaffe, B. (2015). A 2-D process-based model for suspended sediment dynamics: A first step towards ecological modeling. *Hydrology and Earth System Sciences*, *19*(6), 2837–2857. https://doi.org/10.5194/hess-19-2837-2015

Asuncion, R. C., & Lee, M. (2017). Impacts of sea level rise on economic growth in developing Asia (ADB Economics Working Paper Series). Asian Development Bank. Retrieved from https://ideas.repec.org/p/ris/adbewp/0507.html

Atwater, B. F., Conrad, S. G., Dowden, J. N., Hedel, C. W., MacDonald, R. L., & Savage, W. (1979). History, landforms, and vegetation of the estuary's tidal marshes. In T. J. Conomos (Ed.), *San Francisco Bay: The urbanized estuary: Investigations into the Natural History of San Francisco Bay and Delta with reference to the influence of man: Fifty-eighth annual meeting of the Pacific Division/American Association for the Advancement of Sci* (pp. 347–386). San Francisco, CA: AAAS Pacific Division. Retrieved from http://pubs.er.usgs.gov/publication/70156305

Atwater, B. F., Hedel, C. W., & Helley, E. J. (1977). Late Quaternary depositional history, Holocene sea-level changes, and vertical crust movement, southern San Francisco Bay, California (Vol. 1014). US Govt. Print. Off.

Barnard, P. L., Schoellhamer, D. H., Jaffe, B. E., & McKee, L. J. (2013). Sediment transport in the San Francisco Bay coastal system: An overview. *Marine Geology*, *345*, 3–17. https://doi.org/10.1016/j.margeo.2013.04.005

Bever, A. J., & MacWilliams, M. L. (2013). Simulating sediment transport processes in San Pablo Bay using coupled hydrodynamic, wave, and sediment transport models. *Marine Geology*, *345*, 235–253. https://doi.org/10.1016/j.margeo.2013.06.012

Bosboom, J., & Reniers, A. J. H. M. (2014). Displacement-based error metrics for morphodynamic models. *Advances in Geosciences*, *39*(2009), 37–43. https://doi.org/10.5194/adgeo-39-37-2014

Bosboom, J., Reniers, A. J. H. M., & Luijendijk, A. P. (2014). On the perception of morphodynamic model skill. *Coastal Engineering*, *94*, 112–125. https://doi.org/10.1016/j.coastaleng.2014.08.008

Castagno, K. A., Jiménez-Robles, A. M., Donnelly, J. P., Wiberg, P. L., Fenster, M. S., & Fagherazzi, S. (2018). Intense storms increase the stability of tidal bays. *Geophysical Research Letters*, *45*, 5491–5500. https://doi.org/10.1029/2018GL078208

Cloern, J. E., Knowles, N., Brown, L. R., Cayan, D., Dettinger, M. D., Morgan, T. L., et al. (2011). Projected evolution of California's San Francisco Bay-Delta-River system in a century of climate change. *PLoS One*, *6*(9), e24465. https://doi.org/10.1371/journal.pone.0024465

Conomos, T. J., & Peterson, D. H. (1977). Suspended-particle transport and circulation in San Francisco Bay: An overview. In *Estuarine processes: Circulation, Sediments, and transfer of material in the estuary* (pp. 82–97). New York: Academic Press. https://doi.org/10.1016/B978-0-12-751802-2.50014-X

Cooper, J. A. G. (2003). Anthropogenic impacts on estuaries. In *Coastal Zones, Estuaries. Encyclopedia of Life Support Systems (EOLSS)* (pp. 246–262). Oxford, UK: UNESCO, EOLSS Publishers.

Dam, G., van der Wegen, M., Labeur, R. J., & Roelvink, D. (2016). Modeling centuries of estuarine morphodynamics in the Western Scheldt estuary. *Geophysical Research Letters*, *43*, 3839–3847. https://doi.org/10.1002/2015GL066725

de Alegria-Arzaburu, A. R., Williams, J. J., & Masselink, G. (2011). Application of XBeach to model storm response on a macrotidal gravel barrier. *Coastal Engineering Proceedings*, *1*(32), 39. https://doi.org/10.9753/icce.v32.sediment.39

de Vriend, H. J., Capobianco, M., Chesher, T., de Swart, H. E., Latteux, B., & Stive, M. J. F. (1993). Approaches to long-term modelling of coastal morphology: A review. *Coastal Engineering*, *21*(1–3), 225–269. https://doi.org/10.1016/0378-3839(93)90051-9

Deltares (2016). Delft3D-FLOW: Simulation of multi-dimensional hydrodynamic flows and transports phenomena, including sediments. User Manual, Version 3.15, Revision 45038.

Elias, E. P. L., & Hansen, J. E. (2013). Understanding processes controlling sediment transports at the mouth of a highly energetic inlet system (San Francisco Bay, CA). *Marine Geology*, *345*, 207–220. https://doi.org/10.1016/j.margeo.2012.07.003

Elmilady, H. (2016). 3D sediment dynamics in an estuarine strait, (MSc thesis). UNESCO-IHE, Delft, Netherlands.

Erikson, L. H., Wright, S. A., Elias, E., Hanes, D. M., Schoellhamer, D. H., & Largier, J. (2013). The use of modeling and suspended sediment concentration measurements for quantifying net suspended sediment transport through a large tidally dominated inlet. *Marine Geology*, *345*, 96–112. https://doi.org/10.1016/j.margeo.2013.06.001

Fagherazzi, S., Mariotti, G., Wiberg, P. L., & Mcglathery, K. J. (2013). Marsh collapse does not require sea level rise. *Oceanography*, *26*(3), 70–77. https://doi.org/10.5670/oceanog.2013.47

Fleming, K., Johnston, P., Zwartz, D., Yokoyama, Y., Lambeck, K., & Chappell, J. (1998). Refining the eustatic sea-level curve since the last glacial maximum using far- and intermediate-field sites. *Earth and Planetary Science Letters*, *163*(1–4), 327–342. https://doi.org/10.1016/S0012-821X(98)00198-8

Flick, R. E., Murray, J. F., & Ewing, L. C. (2003). Trends in United States tidal datum statistics and tide range. *Journal of Waterway, Port, Coastal, and Ocean Engineering*, *129*(4), 155–164. https://doi.org/10.1061/(ASCE)0733-950X(2003)129:4(155)

Ganju, N. K., Knowles, N., & Schoellhamer, D. H. (2008). Temporal downscaling of decadal sediment load estimates to a daily interval for use in hindcast simulations. *Journal of Hydrology*, *349*(3–4), 512–523. https://doi.org/10.1016/j.jhydrol.2007.11.026

Ganju, N. K., & Schoellhamer, D. H. (2006). Annual sediment flux estimates in a tidal strait using surrogate measurements. *Estuarine, Coastal and Shelf Science*, *69*(1–2), 165–178. https://doi.org/10.1016/j.ecss.2006.04.008

Ganju, N. K., & Schoellhamer, D. H. (2008). Lateral variability of the estuarine turbidity maximum in a tidal strait: Chapter 24. *Proceedings in Marine Science*, *9*, 339–355. https://doi.org/10.1016/S1568-2692(08)80026-5

Ganju, N. K., & Schoellhamer, D. H. (2010). Decadal-timescale estuarine geomorphic change under future scenarios of climate and sediment supply. *Estuaries and Coasts*, *33*(1), 15–29. https://doi.org/10.1007/s12237-009-9244-y

Ganju, N. K., Schoellhamer, D. H., & Jaffe, B. E. (2009). Hindcasting of decadal-timescale estuarine bathymetric change with a tidal-timescale model. *Journal of Geophysical Research*, *114*, F04019. https://doi.org/10.1029/2008JF001191

Ganju, N. K., Schoellhamer, D. H., Warner, J. C., Barad, M. F., & Schladow, S. G. (2004). Tidal oscillation of sediment between a river and a bay: A conceptual model. *Estuarine, Coastal and Shelf Science*, *60*(1), 81–90. https://doi.org/10.1016/J.ECSS.2003.11.020

Gilbert, G. K. (1917). Hydraulic-mining debris in the Sierra Nevada. US Government Printing Office.

Goman, M., & Wells, L. (2000). Trends in River Flow Affecting the Northeastern Reach of the San Francisco Bay Estuary over the Past 7000 Years. *Quaternary Research*, *54*(2), 206–217. https://doi.org/10.1006/QRES.2000.2165

Harvey, J., Coon, D., & Abouchar, J. (1998). Habitat lost: Taking the pulse of estuaries in the Canadian Gulf of Maine.

Hayes, T. P., Kinney, J. J. R., & Wheeler, N. J. M. (1984). California_Surface_Wind_Climatology.

Hoitink, A. J. F., Hoekstra, P., & van Maren, D. S. (2003). Flow asymmetry associated with astronomical tides: Implications for the residual transport of sediment. *Journal of Geophysical Research*, *108*(C10), 3315. https://doi.org/10.1029/2002JC001539

IPCC (2013). In T. F. Stocker, et al. (Eds.), *Climate change 2013: The physical science basis: Working Group I contribution to the fifth assessment report of the Intergovernmental Panel on Climate Change* (p. 1535). Cambridge, UK and New York: Cambridge University Press. https://doi.org/10.1017/CBO9781107415324

Jaffe, B. E., Smith, R. E., & Foxgrover, A. C. (2007). Anthropogenic influence on sedimentation and intertidal mudflat change in San Pablo Bay, California: 1856–1983. *Estuarine, Coastal and Shelf Science*, *73*(1–2), 175–187. https://doi.org/10.1016/j.ecss.2007.02.017

Kemp, A. C., Horton, B. P., Donnelly, J. P., Mann, M. E., Vermeer, M., & Rahmstorf, S. (2011). Climate related sea-level variations over the past two millennia. *Proceedings of the National Academy of Sciences*, *108*(27), 11,017–11,022. https://doi.org/10.1073/pnas.1015619108

Kimmerer, W. (2004). Open water processes of the San Francisco estuary: From physical forcing to biological responses. *San Francisco Estuary and Watershed Science*, *2*(1). Retrieved from http://www.escholarship.org/uc/item/9bp499mv, https://doi.org/10.15447/sfews.2004v2iss1art1

Knowles, N. (2009). Potential inundation due to rising sea levels in the San Francisco Bay region (Draft Pape). Sacramento,CA. Retrieved from http://pubs.er.usgs.gov/publication/70043798

Knowles, N., & Cayan, D. R. (2002). Potential effects of global warming on the Sacramento/San Joaquin watershed and the San Francisco estuary. *Geophysical Research Letters*, *29*(18), 1891. https://doi.org/10.1029/2001GL014339

Kraft, J. C., Yi, H., & Khalequzzaman, M. (1992). Geologic and human factors in the decline of the tidal salt marsh lithosome: the Delaware estuary and Atlantic coastal zone. *Sedimentary Geology*, *80*(3–4), 233–246. https://doi.org/10.1016/0037-0738(92)90043-Q

Krone, R. B. (1979). Sedimentation in the San Francisco Bay system. In T. J. Conomos (Ed.), *San Francisco Bay: The urbanized estuary* (pp. 85–96). San Francisco, CA: American Association for the Advancement of Science.

Krone, R. B. (1996). Recent sedimentation in the San Francisco Bay system. In J. T. Hollibaugh (Ed.), *San Francisco Bay: The ecosystem* (pp. 36–67). San Francisco, CA: Pacific division, American Association for the Advancement of Science.

Kuijper, C., Steijn, R., Roelvink, D., & van der Kaaij, T. (2004). Morphological modelling of the Western Scheldt: Validation of DELFT3D. Delft. Retrieved from http://www.vliz.be/en/imis?refid=103886

Leonardi, N., Carnacina, I., Donatelli, C., Ganju, N. K., Plater, A. J., Schuerch, M., & Temmerman, S. (2018). Dynamic interactions between coastal storms and salt marshes: A review. *Geomorphology*, *301*, 92–107. https://doi.org/10.1016/J.GEOMORPH.2017.11.001

Lesser, G. R. (2009). An approach to medium-term coastal morphological modelling, (PhD thesis). UNESCO-IHE & Delft Technical University, Delft, Netherlands: CRC Press/Balkema.

Lesser, G. R., Roelvink, D., van Kester, J. A. T. M., & Stelling, G. S. (2004). Development and validation of a three-dimensional morphological model. *Coastal Engineering*, *51*(8–9), 883–915. https://doi.org/10.1016/j.coastaleng.2004.07.014

Lewicki, M., & McKee, L. (2010). New methods for estimating annual and long-term suspended sediment loads from small tributaries to San Francisco Bay. *IAHS Publication*, *337*(5), 121–125.

Locke, J. L. (1971). Sedimentation and foraminiferal aspects of the recent sediments of San Pablo Bay, (MS thesis). Fac. of the Dep. of Geol., San Jose State Coll., San Jose, CAL.

MacVean, L., & Lacy, J. R. (2014). Interactions between waves, sediment, and turbulence on a shallow estuarine mudflat. *Journal of Geophysical Research: Oceans*, *119*, 1534–1553. https://doi.org/10.1002/2013JC009477

Martyr-Koller, R. C., Kernkamp, H. W. J., van Dam, A., van der Wegen, M., Lucas, L. V., Knowles, N., et al. (2017). Application of an unstructured 3D finite volume numerical model to flows and salinity dynamics in the San Francisco Bay-Delta. *Estuarine, Coastal and Shelf Science*, *192*, 86–107. https://doi.org/10.1016/J.ECSS.2017.04.024

McKee, L. J., Lewicki, M., Schoellhamer, D. H., & Ganju, N. K. (2013). Comparison of sediment supply to San Francisco Bay from watersheds draining the Bay Area and the Central Valley of California. *Marine Geology*, *345*, 47–62. https://doi.org/10.1016/J.MARGEO.2013.03.003

Mitsch, W. J., & Gosselink, J. G. (2000). The value of wetlands: Importance of scale and landscape setting. *Ecological Economics*, *35*(1), 25–33. https://doi.org/10.1016/S0921-8009(00)00165-8

Moftakhari, H. R., Jay, D. A., Talke, S. A., & Schoellhamer, D. H. (2015). Estimation of historic flows and sediment loads to San Francisco Bay, 1849–2011. *Journal of Hydrology*, *529*, 1247–1261. https://doi.org/10.1016/j.jhydrol.2015.08.043

Murphy, A. H., & Epstein, E. S. (1989). Skill scores and correlation coefficients in model verification. *Monthly Weather Review*, *117*, 572–582. https://doi.org/10.1175/1520-0493(1989)117<0572:SSACCI>2.0.CO;2

Murray, A. B. (2003). Contrasting the goals, strategies, and predictions associated with simplified numerical models and detailed simulations. In *Prediction in geomorphology*, *Geophysical Monograph Series* (Vol. 135, pp. 151–168). Washington, DC: American Geophysical Union. https://doi.org/10.1029/135GM11

National Research Council (2012). *Sea-level rise for the coasts of California, Oregon, and Washington*. Washington, DC: National Academies Press. https://doi.org/10.17226/13389

Nicholls, R. J., & Cazenave, A. (2010). Sea-level rise and its impact on coastal zones. *Science*, *328*(5985), 1517–1520. https://doi.org/10.1126/science.1185782

NOAA. (2018). NOAA Tides & Currents. Retrieved from https://tidesandcurrents.noaa.gov/map/index.shtml?type=active&region=California

Oltmann, R. N. (1996). Sediment inflow to the delta from the Sacramento and San Joaquin Rivers. *Interagency Ecological Program Newsletter*, *9*(2), 22–23. Retrieved from http://pubs.er.usgs.gov/publication/70175203

Oltmann, R. N. (1999). Sediment inflow to the Sacramento-San Joaquin Delta and the San Francisco Bay. *Interagency Ecological Program Newsletter*, *12*(1), 30–33. Retrieved from http://pubs.er.usgs.gov/publication/70175206

Parris, A., Bromirski, P., Burkett, V., Cayan, D., Culver, M., Hall, J., et al. (2012). Global sea level rise scenarios for the US national climate assessment. NOAA Tech Memo OAR CPO-1.

Partheniades, E. (1965). Erosion and deposition of cohesive soils. *Journal of the Hydraulics Division*, *91*(1), 105–139.

Passeri, D. L., Hagen, S. C., Medeiros, S. C., Bilskie, M. V., Alizad, K., & Wang, D. (2015). The dynamic effects of sea level rise on low-gradient coastal landscapes: A review. *Earth's Future*, *3*(6), 159–181. https://doi.org/10.1002/2015EF000298

Pelling, M., & Blackburn, S. (2013). *Megacities and the coast: risk, resilience, and transformation*. London: Routledge. Retrieved from https://www.routledge.com/Megacities-and-the-Coast-Risk-Resilience-and-Transformation/Pelling-Blackburn/p/book/9780415815123

Peri, J., & Šverko, Z. (2015). *Economic Impacts of Sea Level Rise Caused By Climate Change*, *3*, 285–294.

Pethick, J. (1994). Estuaries and wetlands: Function and form. In R. A. Falconer & P. Goodwin (Eds.), *Wetland management* (pp. 75–87). London,UK: Thomas Telford.

Roelvink, D. (2006). Coastal morphodynamic evolution techniques. *Coastal Engineering*, *53*(2–3), 277–287. https://doi.org/10.1016/j.coastaleng.2005.10.015

Rossington, K., & Spearman, J. (2009). Past and future evolution in the Thames Estuary. *Ocean Dynamics*, *59*, 709–718. https://doi.org/10.1007/s10236-009-0207-4

Ruhl, C. A., & Schoellhamer, D. H. (2004). Spatial and temporal variability of suspended-sediment concentrations in a shallow estuarine environment. *San Francisco Estuary and Watershed Science*, *2*(2). https://doi.org/10.15447/sfews.2004v2iss2art1

Sampath, D. M. R., Boski, T., Silva, P. L., & Martins, F. A. (2011). Morphological evolution of the Guadiana estuary and intertidal zone in response to projected sea-level rise and sediment supply scenarios. *Journal of Quaternary Science*, *26*(2), 156–170. https://doi.org/10.1002/jqs.1434

Schoellhamer, D. H., Ganju, N. K., & Shellenbarger, G. G. (2008). Sediment transport in San Pablo Bay. In D. A. Cacchione & P. A. Mull (Eds.), *Technical studies for the aquatic transfer facility: Hamilton wetlands restoration project* (pp. 36–107). San Francisco: U.S. Army Corps of Engineers.

Smith, B. J. (1965). Sedimentation in the San Francisco Bay system. In *Proc. of the Interagency Sedimentation Conference* (pp. 675–708).

Smith, R. (2002). Historical Golden Gate tidal series, NOAA Tech. Rep. NOS CO-OPS 035, U.S. Department of Commerce, Washington, DC.

Sutherland, J., Peet, A. H., & Soulsby, R. L. (2004). Evaluating the performance of morphological models. *Coastal Engineering*, *51*(8–9), 917–939. https://doi.org/10.1016/j.coastaleng.2004.07.015

Takekawa, J. Y., Thorne, K. M., Buffington, K. J., Spragens, K. A., Swanson, K. M., Drexler, J. Z., et al. (2013). Final report for sea-level rise response modeling for San Francisco Bay estuary tidal marshes. US Geological Survey.

Teeter, A. M., Letter, J. V, Jr., Pratt, T. C., Callegan, C. J., & Boyt, W. L. (1997). San Francisco Bay long-term management strategy (LTMS) for dredging and disposal. Report 2. Baywide Suspended Sediment Transport Modeling.

Thorne, K., Macdonald, G., Guntenspergen, G., Ambrose, R., Buffington, K., Dugger, B., et al. (2018). U. S. Pacific coastal wetland resilience and vulnerability to sea-level rise, (February), 1–11. https://doi.org/10.1126/sciadv.aao3270

US EPA (2018). San Francisco Bay Delta: About the watershed. Retrieved from https://www.epa.gov/sfbay-delta/about-watershed

USGS (2018). Water Quality of San Francisco Bay. Retrieved from https://sfbay.wr.usgs.gov/access/wqdata/index.html

van der Wegen, M. (2013). Numerical modeling of the impact of sea level rise on tidal basin morphodynamics. *Journal of Geophysical Research: Earth Surface*, *118*, 447–460. https://doi.org/10.1002/jgrf.20034

van der Wegen, M., Dastgheib, A., Jaffe, B. E., & Roelvink, D. (2011). Bed composition generation for morphodynamic modeling: Case study of San Pablo Bay in California, USA. *Ocean Dynamics*, *61*(2–3), 173–186. https://doi.org/10.1007/s10236-010-0314-2

van der Wegen, M., Jaffe, B., Foxgrover, A., & Roelvink, D. (2016). Mudflat morphodynamics and the impact of sea level rise in South San Francisco Bay. *Estuaries and Coasts*, *40*, 37–49. https://doi.org/10.1007/s12237-016-0129-6.

van der Wegen, M., & Jaffe, B. E. (2013). Towards a probabilistic assessment of process-based, morphodynamic models. *Coastal Engineering*, *75*, 52–63. https://doi.org/10.1016/j.coastaleng.2013.01.009

van der Wegen, M., & Jaffe, B. E. (2014). Processes governing decadal-scale depositional narrowing of the major tidal channel in San Pablo Bay, California, USA. *Journal of Geophysical Research: Earth Surface*, *119*, 1136–1154. https://doi.org/10.1002/2013JF002824

Van der Wegen, M., Jaffe, B. E., & Roelvink, D. (2011). Process-based, morphodynamic hindcast of decadal deposition patterns in San Pablo Bay, California, 1856–1887. *Journal of Geophysical Research*, *116*, F02008. https://doi.org/10.1029/2009JF001614

van der Wegen, M., & Roelvink, D. (2008). Long-term morphodynamic evolution of a tidal embayment using a two-dimensional, process-based model. *Journal of Geophysical Research*, *113*, C03016. https://doi.org/10.1029/2006JC003983

Van Goor, M. A., Zitman, T. J., Wang, Z. B., & Stive, M. J. F. (2003). Impact of sea-level rise on the morphological equilibrium state of tidal inlets. *Marine Geology*, *202*(3–4), 211–227. https://doi.org/10.1016/S0025-3227(03)00262-7

Van Rijn, L. C., Walstra, D. J. R., & Ormondt, M. van. (2004). Description of TRANSPOR2004 and implementation in Delft3D-ONLINE. *Z3748*.

Vroom, J., van der Wegen, M., Martyr-Koller, R. C., & Lucas, L. V. (2017). What determines water temperature dynamics in the San Francisco Bay-Delta system? *Water Resources Research*, *53*, 9901–9921. https://doi.org/10.1002/2016WR020062

Weather2 (2018). San Pablo Bay Climate History. Retrieved from http://www.myweather2.com/City-Town/United-States-Of-America/California/San-Pablo-Bay/climate-profile.aspx?month=12

Werner, B. T. (2003). Modeling landforms as self-organized, hierarchical dynamical systems. In P. R. Wilcock & R. M. Iverson (Eds.), *Prediction in geomorphology*, *Geophysical Monograph Series* (Vol. 135, pp. 133–150). Washington, DC: American Geophysical Union. https://doi.org/10.1029/135GM10

Windfinder (2018). Wind, wave & weather reports, forecasts & statistics worldwide. Retrieved from https://www.windfinder.com/#12/38.0351/-122.3273

Winterwerp, J. c., & Van Kesteren, W. G. M. (2004). Settling and sedimentation. In J. C. Winterwerp & W. G. M. van Kesteren (Eds.), *Introduction to the physics of cohesive sediment in the marine environment* (Vol. 56, pp. 121–159). Amsterdam: Elsevier. https://doi.org/10.1016/S0070-4571(04)80006-2

Wright, S. a., & Schoellhamer, D. H. (2004). Trends in the sediment yield of the Sacramento River, California, 1957–2001. *San Francisco Estuary and Watershed Science*, *14*(1), 1–10. https://doi.org/10.5811/westjem.2011.5.6700

Zhou, X., Zheng, J., Doong, D.-J., & Demirbilek, Z. (2013). Sea level rise along the East Asia and Chinese coasts and its role on the morphodynamic response of the Yangtze River estuary. *Ocean Engineering*, *71*, 40–50. https://doi.org/10.1016/J.OCEANENG.2013.03.014

Zhou, Z., Coco, G., van der Wegen, M., Gong, Z., Zhang, C., & Townend, I. (2015). Modeling sorting dynamics of cohesive and non-cohesive sediments on intertidal flats under the effect of tides and wind waves. *Continental Shelf Research*, *104*, 76–91. https://doi.org/10.1016/J.CSR.2015.05.010